

Energy spectra in p -shell Λ hypernuclei and ${}^{19}_{\Lambda}\text{F}$ and spin-dependent ΛN interactions

Yoshiko Kanada-En'yo

Department of Physics, Kyoto University, Kyoto 606-8502, Japan

Masahiro Isaka

Research Center for Nuclear Physics (RCNP), Osaka University, Ibaraki, Osaka, 567-0047, Japan

Toshio Motoba

*Laboratory of Physics, Osaka Electro-Communication University, Neyagawa 572-8530, Japan and
Yukawa Institute for Theoretical Physics, Kyoto University, Kyoto 606-8502, Japan*

Energy spectra of $0s$ -orbit Λ states in p -shell Λ hypernuclei (${}^A_{\Lambda}Z$) and those in ${}^{19}_{\Lambda}\text{F}$ are studied with the microscopic cluster model and antisymmetrized molecular dynamics using the G -matrix effective ΛN (ΛNG) interactions. Spin-dependent terms of the ESC08a version of the ΛNG interactions are tested and phenomenologically tuned to reproduce observed energy spectra in p -shell ${}^A_{\Lambda}Z$. Spin-dependent contributions of the ΛN interactions to spin-doublet splitting and excitation energies are discussed. Energy spectra for unobserved excited states in p -shell ${}^A_{\Lambda}Z$ and ${}^{19}_{\Lambda}\text{F}$ are predicted with the modified ΛNG interactions.

I. INTRODUCTION

In this decade, experimental and theoretical studies of hypernuclei have remarkably progressed. For Λ hypernuclei, experimental studies with high-resolution γ -ray measurements have been extensively performed to provide detailed information of energy spectra in the p -shell region [1–3]. The γ -ray spectroscopic study of sd -shell ${}^A_{\Lambda}Z$ has just started, and the observed spectra in ${}^{19}_{\Lambda}\text{F}$ have been reported [4]. The observed energy spectra are useful information for study of ΛN interactions. In particular, energy splittings between the spin-doublet $J_{>} = I + 1/2$ and $J_{<} = I - 1/2$ states with the Λ -spin coupling in parallel and anti-parallel to the core nuclear spin I are sensitive probes to figure out spin dependences of the ΛN interactions in Λ hypernuclei. Based on compilation of the precise data updated recently, it is time to comprehensively understand the energy spectra in p -shell ${}^A_{\Lambda}Z$ with theoretical study. Moreover, it is able to test spin dependences of the ΛN interactions in comparison of calculated spectra with observed data.

Structure studies of p -shell Λ hypernuclei have been performed with various theoretical models such as cluster models [5–22], shell models (SM) [23–28], mean-field and beyond mean-field models [29–38], hyper antisymmetrized molecular dynamics (HAMD) model [39–43], and no-core shell model [44], and so on. Spin-dependent ΛN interactions have been discussed in details in systematic studies for various p -shell ${}^A_{\Lambda}Z$, for instance, with cluster-model [12, 14–16] and shell-model calculations [26–28].

In the structure calculations of Λ hypernuclei, YN interactions developed based on the meson-theoretical models by the Nijmegen group have been widely used. After many trials and continuous improvements, new versions (ESC08 series) of the extended-soft-core (ESC) model of the YN interactions have been proposed [45–47]. The spin-independent part of the ESC08(a,b) ΛN

interaction was tested and found to be reasonable in description of Λ binding energies in a wide mass number region [42, 43, 47]. However, in spin dependences of the ESC08(a,b), problems were found in reproducing the observed spin-doublet splitting energies [47]. It is a demanded issue to test the spin dependences of the ESC08 with systematic investigation of energy spectra in p -shell ${}^A_{\Lambda}Z$ and consider possible modification of the spin-dependent ΛN interactions in comparison with the experimental data.

It is known from observed Λ binding energies that the ΛN interactions are weak compared with the NN interactions. Moreover, from observed energy spectra, the spin-dependent ΛN interactions have been found to be rather weak compared with the spin-independent ΛN interactions, and therefore, they may give perturbative contributions to structures of ${}^A_{\Lambda}Z$. It means that the Λ particle in ${}^A_{\Lambda}Z$, an impurity embedded in nuclear system, is regarded as a spectator probing the ΛN interactions. In particular, energy spectra of $(0s)_{\Lambda}$ states can be a good probe that detects rather directly the spin-dependent ΛN interactions through the spin-dependent mean-field potential for the $0s$ -orbit Λ determined by nuclear spin structure in core nuclei. In order to describe detailed energy spectra and understand properties of the spin-dependent ΛN interactions, one needs a reliable structure model which can properly describe nuclear structures, particularly, nuclear spin configurations. Furthermore, for systematic studies of p -shell ${}^A_{\Lambda}Z$, it is also demanded to describe cluster structures in light-mass p -shell nuclei. Cluster models can respond to the latter demand, but in general they are not sufficient in describing nuclear spin configurations in med- p -shell nuclei because cluster breakings are not taken into account in the model. Shell models are useful to investigate detailed spin configurations, but it is not suitable to deal with remarkable clustering as well as nuclear deformations because of limitation of the model space. The antisymmetrized molecular dynamics (AMD) model [48–51] is one of use-

ful tools for systematic study of p -shell and sd -shell nuclei because it can describe cluster and spin structures in the ground and excited states of general nuclei. A version of the AMD model, variation after projection called AMD+VAP, has been applied to various p -shell nuclei including odd-odd nuclei and proved to be successful in describing nuclear spin properties such as μ moments, $M1$, and GT transitions [51–54]. The HAMD, which is another version of the AMD applied to Λ hypernuclei by one of the authors (M. I.) and his collaborators [39–43], is also a promising approach for study of spin-dependent ΛN interactions though its application is still limited.

The aim of the present work is to investigate energy spectra in p -shell ${}^A_\Lambda Z$ and discuss spin dependences of the ΛN interactions with microscopic structure model calculations. In the previous works by one of the authors (Y. K-E.), spin-averaged energy spectra of low-lying $(0s)_\Lambda$ states have been investigated by applying the cluster model for core nuclei and a single-channel potential model for a Λ particle with the spin-independent effective ΛN interactions [55]. In order to calculate energy spectra of ${}^A_\Lambda Z$ with spin-dependent effective ΛN interactions, here we apply the AMD+VAP model in addition to the microscopic cluster model. The spin-dependent ΛN interactions are perturbatively treated in the AMD+VAP calculation. Comparing the calculated spin-doublet splitting energies with observed data in p -shell ${}^A_\Lambda Z$, we test spin dependences of the G -matrix effective ΛN (ΛNG) interactions of the ESC08a model [45–47]. A modification of the ESC08a ΛNG interaction is proposed by phenomenological tuning of the spin-dependent terms to adjust available data of energy spectra. Using the modified ΛNG interactions, the spin-dependent contributions of the ΛN interactions to energy spectra are investigated. In addition, theoretical spectra for unknown excited states in p -shell ${}^A_\Lambda Z$ and ${}^{19}_\Lambda\text{F}$ are predicted.

This paper is organized as follows. In the next section, we explain the framework of the present calculation. The effective NN and ΛN interactions are explained in Sec. III. Structure properties of core nuclei ${}^{A-1}Z$ are shown in Sec. IV. In Sec. V, results for ${}^A_\Lambda Z$ and the modification of the spin-dependent ΛN interactions are given. The paper is summarized in Sec. VI. In appendixes A and B, validity of the folding potential model approximation and spin rearrangement effects are discussed, respectively.

II. FRAMEWORK

We apply two models to describe structures of core nuclear part. One is the microscopic cluster model with the generator coordinate method (GCM) [56, 57], which has been used in the previous works [55, 58], and the other is the AMD+VAP. The framework of the AMD model is explained, for example, in Ref. [51]. For details of the frameworks, see those papers and references therein.

In the cluster model with the GCM, the dynamical inter-cluster motion is taken into account by means of superposition of cluster wave functions having various inter-cluster distances. However, the cluster model contains only a part of intrinsic-spin configurations because it ignores cluster breaking. To overcome this problem of the cluster model and investigate spin-dependent contributions of the ΛN interactions to energy spectra, we apply the AMD model. A basis AMD wave function is given by a Slater determinant of single-nucleon Gaussian wave functions, in which Gaussian centroids and intrinsic-spin orientations of all nucleons are independently treated as variational parameters. The AMD model does not rely on *a priori* assumption of clusters and can describe the cluster breaking and cluster formation. Compared with the cluster model, the AMD is a flexible model, in particular, for intrinsic-spin degrees of freedom. However, in description of dynamical inter-cluster motion, the present AMD+VAP calculation is more limited than the cluster model because only a few AMD configurations are superposed.

The ΛN interactions contain spin-independent (V_0) and spin-dependent (V_1) parts as,

$$V_{\Lambda N} = V_0 + V_1. \quad (1)$$

The spin-independent part (V_0) is dominant and gives leading contributions, whereas the spin-dependent part (V_1) is relatively weak. In the present calculation, we first consider the spin-independent ΛN interaction V_0 as the leading part for the mean potential of the $0s$ -orbit Λ , and then perturbatively take into account the spin-dependent ΛN interaction V_1 . For p -shell ${}^A_\Lambda Z$, we investigate the leading contributions with cluster and AMD models using only V_0 by ignoring the spin dependence of the ΛN interactions. In order to investigate the spin-dependent contributions from V_1 , we apply the AMD model. For ${}^{19}_\Lambda\text{F}$, we investigate the leading and perturbative contributions with the microscopic cluster model of ${}^{16}\text{O}+p+n$.

A. Calculations of core nuclei with microscopic structure models

1. Cluster model with GCM for p -shell nuclei

Core nuclei ${}^{A-1}Z$ in ${}^A_\Lambda Z$ are calculated with the microscopic cluster model in the same way as the previous calculations for p -shell Λ and double- Λ hypernuclei in Refs. [55, 58]. In the model, microscopic A_N -nucleon wave functions are expressed by the Brink-Bloch cluster wave functions [59] and superposed by means of the GCM. Here, $A_N = A - 1$ is the mass number of core nuclei. The cluster wave functions of $\alpha + d$, $\alpha + t$, 2α , $2\alpha + n$, $2\alpha + p$, $2\alpha + n^2$, $2\alpha + d$, $2\alpha + t$, $2\alpha + h$, 3α , and $3\alpha + h$ cluster wave functions are adopted for ${}^6\text{Li}$, ${}^7\text{Li}$, ${}^8\text{Be}$, ${}^9\text{Be}$, ${}^9\text{B}$, ${}^{10}\text{Be}$, ${}^{10}\text{B}$, ${}^{11}\text{B}$, ${}^{11}\text{C}$, ${}^{12}\text{C}$, and ${}^{15}\text{O}$ systems, respectively. d , n^2 , t , h , and α clusters are written by harmonic oscillator (h.o.) $0s$ configurations. For

^{10}Be , ^{11}B , ^{11}C , and ^{12}C , additional configurations are included in the model space to take into account cluster breaking components as explained in Ref. [58]. Namely, the $^6\text{He} + \alpha$ wave functions [60] are added to the $2\alpha + n^2$ wave functions for ^{10}Be , and the $p_{3/2}$ configurations are added to the $2\alpha + t$, $2\alpha + h$, and 3α cluster wave functions for ^{11}B , ^{11}C and ^{12}C [55, 61]. Those cluster models (with and without additional configurations) are denoted by the label “CL” in the paper. The h.o. width parameter ν of clusters is commonly chosen as $\nu = 0.235 \text{ fm}^{-2}$ for $A_N \leq 12$ nuclei. For ^{15}O , the value $\nu = 0.16 \text{ fm}^{-2}$ which reproduces the nuclear size of the p -closed ^{16}O is used.

The Brink-Bloch cluster wave function for a A_N -nucleon system consisting of C_1, \dots, C_k clusters is denoted as $\Phi_{\text{BB}}(\mathbf{S}_1, \dots, \mathbf{S}_k)$ with the parameters \mathbf{S}_j ($j = 1, \dots, k$) of cluster center positions. k is the number of clusters. To take into account inter-cluster motion, the GCM is applied to the angular-momentum and parity projected Brink-Bloch cluster wave functions with respect to the generator coordinates \mathbf{S}_j . The wave function $\Psi_N(I_n^\pi)$ for the nuclear angular momentum and parity I_n^π state is given by a linear combination of the Brink-Bloch wave functions with various configurations of $\{\mathbf{S}_1, \dots, \mathbf{S}_k\}$ as

$$\Psi_N(I_n^\pi) = \sum_{\mathbf{S}_1, \dots, \mathbf{S}_k} \sum_K c_{\mathbf{S}_1, \dots, \mathbf{S}_k, K}^{I_n^\pi} P_{MK}^{I_n^\pi} \Phi_{\text{BB}}(\mathbf{S}_1, \dots, \mathbf{S}_k), \quad (2)$$

where $P_{MK}^{I_n^\pi}$ is the angular momentum and parity projection operator. The coefficients $c_{\mathbf{S}_1, \dots, \mathbf{S}_k, K}^{I_n^\pi}$ are determined by solving Griffin-Hill-Wheeler equations [56, 57], which is equivalent to the diagonalization of the Hamiltonian and norm matrices,

$$\begin{aligned} & \langle \Phi_{\text{BB}}(\mathbf{S}_1, \dots, \mathbf{S}_k) | P_{MK}^{I_n^\pi} | H_N | P_{MK'}^{I_n^\pi} \Phi_{\text{BB}}(\mathbf{S}'_1, \dots, \mathbf{S}'_k) \rangle, \\ & \langle \Phi_{\text{BB}}(\mathbf{S}_1, \dots, \mathbf{S}_k) | P_{MK}^{I_n^\pi} | P_{MK'}^{I_n^\pi} \Phi_{\text{BB}}(\mathbf{S}'_1, \dots, \mathbf{S}'_k) \rangle. \end{aligned}$$

Here H_N is the Hamiltonian of the nuclear part described later.

For the $\alpha + d$ and 2α wave functions, \mathbf{S}_1 and \mathbf{S}_2 are chosen to be $\mathbf{S}_1 - \mathbf{S}_2 = (0, 0, d)$ with the generator coordinate $d = \{1, 2, \dots, 15 \text{ fm}\}$ of the inter-cluster distance. For the $\alpha + t$ wave functions, $d = \{1, 2, \dots, 8 \text{ fm}\}$ are adopted to obtain a bound state solution for the resonance state $^7\text{Li}(7/2_-^-)$ corresponding to a bound state approximation. For configurations of $2\alpha + n^2$, $2\alpha + d$, $2\alpha + t$, $2\alpha + h$, and 3α cluster wave functions, $\mathbf{S}_{1,2,3}$ are chosen to be

$$\mathbf{S}_1 - \mathbf{S}_2 = (0, 0, d), \quad (3)$$

$$\mathbf{S}_3 - \frac{A_2 \mathbf{S}_1 + A_1 \mathbf{S}_2}{A_1 + A_2} = (r \sin \theta, 0, r \cos \theta), \quad (4)$$

with $d = \{1.2, 2.2, \dots, 4.2 \text{ fm}\}$, $r = \{0.5, 1.5, \dots, 4.5 \text{ fm}\}$, and $\theta = \{0, \pi/8, \dots, \pi/2\}$. Here A_i is the mass number of the C_i cluster. For $2\alpha + n(p)$ configurations, $d = \{1.2, 2.2, \dots, 6.2 \text{ fm}\}$, $r = \{0.5, 1.5, \dots, 6.5 \text{ fm}\}$, and

$\theta = \{0, \pi/8, \dots, \pi/2\}$ are used to describe remarkable clustering in $^9\text{Be}(^9\text{B})$. For ^{15}O , the $3\alpha + h$ configurations are restricted to be pyramid configurations with a regular triangle 3α and a h cluster on the vertical axis passing through the center of the 3α plane. The side d of the triangle and the height r are chosen to be $d = \{0.5, 1.5, \dots, 3.5 \text{ fm}\}$ and $r = \{0.5, 1.5, \dots, 4.5 \text{ fm}\}$.

2. AMD+VAP for p -shell nuclei

The AMD+VAP method is applied for p -shell nuclei to investigate contributions of the spin-dependent ΛN interactions in A_Z . In the AMD framework, a basis wave function is given by a Slater determinant

$$\Phi_{\text{AMD}}(\mathbf{Z}) = \frac{1}{\sqrt{A_N!}} \mathcal{A}\{\varphi_1, \varphi_2, \dots, \varphi_{A_N}\}, \quad (5)$$

where \mathcal{A} is the antisymmetrizer, and φ_i is the i th single-particle wave function written by a product of spatial, spin, and isospin wave functions,

$$\varphi_i = \phi_{\mathbf{X}_i} \chi_i \tau_i, \quad (6)$$

$$\phi_{\mathbf{X}_i}(\mathbf{r}_j) = \left(\frac{2\nu}{\pi}\right)^{3/4} \exp[-\nu(\mathbf{r}_j - \mathbf{X}_i)^2], \quad (7)$$

$$\chi_i = \left(\frac{1}{2} + \xi_i\right) \chi_\uparrow + \left(\frac{1}{2} - \xi_i\right) \chi_\downarrow, \quad (8)$$

where $\phi_{\mathbf{X}_i}$ and χ_i are the spatial and intrinsic-spin functions, respectively, and τ_i is the isospin function fixed to be proton or neutron. The width parameter ν is chosen to be the same value as that used in the cluster model. The AMD wave function is specified by a parameter set $\mathbf{Z} \equiv \{\mathbf{X}_1, \dots, \mathbf{X}_{A_N}, \xi_1, \dots, \xi_{A_N}\}$. The Gaussian centroids \mathbf{X}_i and intrinsic-spin orientations ξ_i of all nucleons are independently treated as variational parameters in the energy variation. Owing to the flexibility of spatial and intrinsic-spin configurations of single-nucleon Gaussian wave packets, the AMD wave function can express various cluster structures with cluster breaking degrees of freedom as well as various intrinsic spin configurations. Moreover, it can also describe shell-model wave functions because of the antisymmetrization.

In the AMD+VAP, the energy variation is done after the angular-momentum and parity projections in the AMD model space as

$$\frac{\delta}{\delta \mathbf{X}_i} \frac{\langle \Psi_N(I^\pi) | H_N | \Psi_N(I^\pi) \rangle}{\langle \Psi_N(I^\pi) | \Psi_N(I^\pi) \rangle} = 0, \quad (9)$$

$$\frac{\delta}{\delta \xi_i} \frac{\langle \Psi_N(I^\pi) | H_N | \Psi_N(I^\pi) \rangle}{\langle \Psi_N(I^\pi) | \Psi_N(I^\pi) \rangle} = 0, \quad (10)$$

$$\Psi_N(I^\pi) = P_{MK}^{I^\pi} \Phi_{\text{AMD}}(\mathbf{Z}), \quad (11)$$

in order to obtain the optimum solution of the parameter set \mathbf{Z} for the lowest I^π states. For higher I^π states, the VAP is done for the component orthogonal to the lower I^π states already obtained by the VAP. The method is a version of the AMD and usually called the AMD+VAP. In this paper, it is simply denoted as the AMD.

3. Microscopic three-body model for ^{18}F

For ^{18}F , we use the microscopic $^{16}\text{O} + p + n$ wave functions adopted in the previous study of ^{18}F [62]. The wave functions are written in the form of the Brink-Bloch cluster wave functions for $C_1 = p$, and $C_2 = n$, and $C_3 = ^{16}\text{O}$ and are superposed with the GCM. The same parametrization of the generator coordinates as Ref. [62] is used,

$$\mathbf{S}_1 = (iq_x, r_y, 8D/9), \quad (12)$$

$$\mathbf{S}_2 = (-iq_x, -r_y, 8D/9), \quad (13)$$

$$\mathbf{S}_3 = (0, 0, -D/9). \quad (14)$$

In the present calculation, $D = \{1, 2, \dots, 7 \text{ fm}\}$ are chosen. For all D values, the coordinate set $(q_x, r_y) = (0, 0)$ is used corresponding to the d cluster. In addition, $q_x = \{0.5, 1, 1.5, 2 \text{ fm}\}$ and $r_y = \{0, 1 \text{ fm}\}$ are used for $D = 2 \text{ fm}$ and $q_x = \{1, 2 \text{ fm}\}$ and $r_y = \{0, 1 \text{ fm}\}$ are used for $D = 3, 4, 5 \text{ fm}$ to take into account the d -cluster breaking at the nuclear surface by the nuclear spin-orbit interactions from ^{16}O . In the total angular momentum projection $P_{MK}^{J\pi}$, $|K| = 1$ components are adopted. Higher $|K|$ states are not included to save computational costs in numerical integration of the Euler angles in the projection. The wave functions are automatically projected onto the isospin $T = 0$ eigen states because of the $|K| = 1$ projection.

The inert ^{16}O cluster is assumed in the $^{16}\text{O} + p + n$ model. In order to see possible 4α -cluster vibration effect in ^{16}O , a $4\alpha + p + n$ model is also applied in the calculation of the leading V_0 contribution. We use the label “CL” for the former model ($^{16}\text{O} + p + n$) with the inert ^{16}O cluster and CL- 4α for the latter one ($4\alpha + p + n$) with the ^{16}O vibration. In the CL- 4α model, regular tetrahedral 4α configurations with the length of a side $r = 0.5, 1.5, 2.5 \text{ fm}$ are adopted in the GCM. As shown later, the vibration effect is found to be minor.

4. Nuclear energy and density

The Hamiltonian of the nuclear part consists of the kinetic terms, effective NN interactions, and Coulomb interactions as follows,

$$H_N = \sum_i^{A_N} \frac{1}{2m_N} \mathbf{p}_i^2 - T_G + \sum_{i < j}^{A_N} V_{NN}(i, j) + \sum_{i < j}^Z V_{\text{coulomb}}(r_{ij}) \quad (15)$$

where T_G is the center of mass (cm) kinetic energy, V_{NN} is the effective NN interactions, and V_{coulomb} is the Coulomb interaction in the A_N -nucleon system. The nuclear energy $E_N = \langle \Psi_N(I_n^\pi) | H_N | \Psi_N(I_n^\pi) \rangle$ and nuclear density $\rho_N^{I_n^\pi}(r)$ are calculated for the nuclear wave functions $\Psi_N(I_n^\pi)$ (normalized as $|\langle \Psi_N(I_n^\pi) | \Psi_N(I_n^\pi) \rangle| = 1$) obtained with the CL and AMD models. In the calculation of the nuclear energy and density, the cm motion of

core nuclei is removed exactly and the radial coordinate r in $\rho_N^{I_n^\pi}(r)$ is defined by the distance from the cm of core nuclei.

B. Λ single-particle state with folding potential model in Λ hypernuclei

1. Λ wave function

The Λ wave functions in Λ hypernuclei are calculated by assuming a $0s$ -orbit Λ within a folding potential model as done in the previous work [55]. In the folding potential model, the Λ -nucleus potential is obtained by folding the spin-independent ΛN central interactions (V_0) with the nuclear density $\rho_N^{I_n^\pi}$. The single-particle Hamiltonian $h_{\Lambda,0}$ for a $0s$ -orbit Λ around the core is given as

$$h_{\Lambda,0} = \frac{1}{2\mu_\Lambda} p_r^2 + U_0(\rho_N^{I_n^\pi}; r), \quad (16)$$

$$\mu_\Lambda = \frac{(A-1)m_N m_\Lambda}{(A-1)m_N + m_\Lambda}. \quad (17)$$

The nuclear density matrix in the exchange potential is approximated with the density matrix expansion in the local density approximation [63] as done in the previous works. For a given nuclear density $\rho_N^{I_n^\pi}(r)$ of the core nucleus I_n^π state, the single-particle energy $\varepsilon_{\Lambda,0}(\rho_N^{I_n^\pi})$ and wave function $\phi_{\Lambda,0}(\rho_N^{I_n^\pi}; r)$ are calculated with the Gaussian expansion method [64, 65]. In Appendix A, we compare the approximately calculated Λ -potential energies $\langle \phi_{\Lambda,0} | U_0(\rho) | \phi_{\Lambda,0} \rangle$ in $^7_\Lambda\text{Li}(I^\pi = 1^+, 3^+)$ with those of the microscopically calculated values $\langle \Psi_N(I^\pi) \phi_{\Lambda,0} | V_0 | \Psi_N(I^\pi) \phi_{\Lambda,0} \rangle$. It is found that the approximation in the exchange potential gives only minor contribution to energy spectra.

In the cluster model calculation of $^A_\Lambda Z$ with $A \leq 13$, we take into account the core polarization, i.e., the nuclear size change induced by the Λ through the spin-independent ΛN central interactions (V_0) in the same way as done in the previous works. It should be commented that, in the previous works, the core polarization in $A > 10$ hypernuclei was found to be small and gives only minor effect to energy spectra. The core polarization is omitted in the cluster model calculation of $^{16}_\Lambda\text{O}$ and $^{19}_\Lambda\text{F}$ for simplicity. In the AMD calculation, we adopt the frozen core approximation without the core polarization. Namely, we omit the core polarization and use the nuclear wave functions obtained for isolate ^{A-1}Z systems without the Λ .

C. Energy contributions of spin-dependent ΛN interactions

Energy contributions of the spin-dependent part V_1 of the ΛN interactions in $^A_\Lambda Z(J^\pi)$ are perturbatively calculated as $\langle \Psi_{^A_\Lambda Z}(J^\pi) | V_1 | \Psi_{^A_\Lambda Z}(J^\pi) \rangle$ by using the unpertur-

bative A -body microscopic wave functions

$$\Psi_{\Lambda Z}(J^\pi) = [\Psi_N(I_n^\pi) \phi_{\Lambda,0} \chi_\Lambda]_J, \quad (18)$$

obtained with V_0 . Here χ_Λ is the Λ -spin function coupling with the nuclear spin I to the total angular momentum J . In the present perturbative treatment, modification of the Λ wave function by V_1 is omitted. Moreover, rearrangement of spin configurations by the V_1 contribution is ignored. We checked the spin rearrangement effect to energy spectra and found that it is mostly minor unless energies of two J^π states for different I^π are close to each other.

D. Calculation procedure

The procedures of the present calculation are summarized below. The calculation is done in three steps as follows.

1. Calculation of the core nuclear part is performed with two kinds of structure models, cluster and AMD models. (For ^{19}F , two kinds of cluster model calculations are done.) The nuclear wave function $\Psi_N(I^\pi)$, nuclear energy $E_N(I^\pi)$, and nuclear density $\rho_N^{I^\pi}(r)$ for $^{A-1}Z(I^\pi)$ are obtained with the Hamiltonian given by Eq. (15).
2. Using the nuclear density $\rho_N^{I^\pi}$ obtained in the first step, the $0s$ -orbit Λ state in ${}^A_\Lambda Z$ is calculated by the folding potential model with the spin-independent part V_0 of the ΛN interactions. The Λ single-particle energy $\varepsilon_{\Lambda,0}(\rho_N^{I^\pi})$ and the Λ wave function $\phi_{\Lambda,0}(\rho_N^{I^\pi})$ are obtained with the Hamiltonian given by Eq. (16). The core polarization is taken into account in the cluster model calculations of ${}^A_\Lambda Z$ with $A \leq 13$. It is omitted in other calculations.
3. The energy contributions from the spin-dependent part V_1 of the ΛN interactions are perturbatively calculated with the unperturbative wave functions $\Psi_{\Lambda Z}(J^\pi)$ given by $\Psi_N(I_n^\pi)$ and $\phi_{\Lambda,0}$, which are obtained in the first and second steps, respectively. The spin rearrangement and $\phi_{\Lambda,0}$ change induced by V_1 are ignored. The third step calculation is done by using the nuclear wave functions $\Psi_N(I_n^\pi)$ obtained with the AMD (for ^{19}F , that with the cluster model).

E. Energies

The ΛN interactions ($V_{\Lambda N}$) contains the spin-independent part (V_0) and the spin-dependent part (V_1). We take into account four spin-dependent terms of V_1 as

$$V_1 = V_\sigma + V_{S_\Lambda} + V_{S_N} + V_T, \quad (19)$$

where V_σ , V_{S_Λ} , V_{S_N} , and V_T are the spin-spin ($\sigma_\Lambda \cdot \sigma_N$), the Λ -spin spin-orbit ($\mathbf{l} \cdot \mathbf{s}_\Lambda$), the nucleon-spin spin-orbit ($\mathbf{l} \cdot \mathbf{s}_N$), and the tensor (S_{12}) terms, respectively. Following the notation usually used in the shell model (SM) calculations [26–28], we denote the contributions from V_σ , V_{S_Λ} , V_{S_N} , and V_T terms as the Δ_σ , S_Λ , S_N , and T contributions, respectively. The $\Lambda\Sigma$ contribution from the $\Lambda\Sigma$ coupling is ignored in the present calculation. In this section, we explain definitions of energies and respective contributions.

1. Total energy and excitation energy

The total energy of ${}^A_\Lambda Z$ is given as

$$E_{\Lambda Z}(J^\pi) = E_N(I^\pi) + \varepsilon_{\Lambda,0}(\rho_N^{I^\pi}) + \langle \Psi_{\Lambda Z}(J^\pi) | V_1 | \Psi_{\Lambda Z}(J^\pi) \rangle. \quad (20)$$

We regard the sum of the first and second terms as the leading term contributed from V_0 and the third term as the perturbative term from V_1 . In the present paper, we evaluate energies of ${}^A_\Lambda Z$ in two ways as follows. In the first calculation, we evaluate both the leading and the perturbative terms with the AMD model calculation as

$$E_{\Lambda Z}(J^\pi) = E_N^{\text{AMD}}(I^\pi) + \varepsilon_{\Lambda,0}^{\text{AMD}}(\rho_N^{I^\pi}) + \langle \Psi_{\Lambda Z}^{\text{AMD}}(J^\pi) | V_1 | \Psi_{\Lambda Z}^{\text{AMD}}(J^\pi) \rangle, \quad (21)$$

where E_N^{AMD} , $\varepsilon_{\Lambda,0}^{\text{AMD}}$, and $\Psi_{\Lambda Z}^{\text{AMD}}$ are the nuclear energy, Λ single-particle energy, and ${}^A_\Lambda Z$ wave function obtained by the AMD. This is a consistent calculation, in which the V_0 and V_1 contributions are calculated with the AMD. However, inter-cluster motion is not necessarily described sufficiently in the present AMD calculation because of the number of basis wave functions is limited as mentioned previously. The inter-cluster motion may give important contributions, in particular, to the leading term. Therefore, we also adopt an alternative way of energy evaluation by replacing the leading terms with those obtained by the CL calculation as

$$E_{\Lambda Z}(J^\pi) = E_N^{\text{CL}}(I^\pi) + \varepsilon_{\Lambda,0}^{\text{CL}}(\rho_N^{I^\pi}) + \langle \Psi_{\Lambda Z}^{\text{AMD}}(J^\pi) | V_1 | \Psi_{\Lambda Z}^{\text{AMD}}(J^\pi) \rangle, \quad (22)$$

which we call the “CL+AMD” calculation. Here E_N^{CL} and $\varepsilon_{\Lambda,0}^{\text{CL}}$ are the nuclear energy and Λ single-particle energy obtained by the CL with V_0 .

In both the AMD and CL+AMD calculations, excitation energies are given by the energy difference between the ground and excited states as

$$E_x(J^\pi) = E_{\Lambda Z}(J^\pi) - E_{\Lambda Z}(\text{gs}). \quad (23)$$

2. The spin-averaged energies

The spin-averaged energy $\bar{E}_{\Lambda Z}(I^\pi)$ is defined by the energy averaged for the spin-doublet partners $J^\pi_>$ and $J^\pi_<$

in ${}^A_\Lambda Z$ states for the core ${}^{A-1}Z(I^\pi)$ state. It is given by sum of the leading and perturbative terms corresponding to the V_0 and V_1 contributions as

$$\bar{E}_{\Lambda Z}(I^\pi) = \bar{E}_{\Lambda Z,0}(I^\pi) + \langle V_{S_N} \rangle_{\Lambda Z}(I^\pi), \quad (24)$$

$$\bar{E}_{\Lambda Z,0}(I^\pi) = E_N(I^\pi) + \varepsilon_{\Lambda,0}(\rho_N^{I^\pi}), \quad (25)$$

$$\langle V_{S_N} \rangle_{\Lambda Z}(I^\pi) = \langle \Psi_{\Lambda Z}(J^\pi) | V_{S_N} | \Psi_{\Lambda Z}(J^\pi) \rangle. \quad (26)$$

The perturbative term is contributed by the S_N term of the spin-dependent ΛN interactions (V_{S_N} in V_1). Note that, in the present calculation without the spin rearrangement, the S_N contribution has no Λ -spin dependence and depends only on the core nuclear spin I^π . The spin-averaged binding energy $\bar{B}_{\Lambda Z}(I^\pi)$ is given by the sum of leading and perturbative terms as

$$\bar{B}_\Lambda(I^\pi) = \bar{B}_{\Lambda,0}(I^\pi) + \bar{B}_{\Lambda,S_N}(I^\pi), \quad (27)$$

$$\bar{B}_{\Lambda,0}(I^\pi) = E_{A-1Z}(I^\pi) - \bar{E}_{\Lambda Z,0}(I^\pi), \quad (28)$$

$$\bar{B}_{\Lambda,S_N}(I^\pi) = -\langle V_{S_N} \rangle_{\Lambda Z}(I^\pi), \quad (29)$$

where $\bar{B}_{\Lambda,0}$ and \bar{B}_{Λ,S_N} are the V_0 and S_N contributions to \bar{B}_Λ , respectively. The spin-averaged excitation energy $\bar{E}_x(I^\pi)$ is defined as

$$\bar{E}_x(I^\pi) = \bar{E}_{\Lambda Z}(I^\pi) - \bar{E}_{\Lambda Z}(\text{gs}). \quad (30)$$

We define the spin-averaged excitation energy shift $\delta_\Lambda(\bar{E}_x)$ induced by the Λ in ${}^A_\Lambda Z$ by the difference from the original excitation energy $E_x({}^{A-1}Z)$ in the ordinary nucleus ${}^{A-1}Z$ as

$$\delta_\Lambda(\bar{E}_x(I^\pi)) = \bar{E}_x(I^\pi) - E_x({}^{A-1}Z; I^\pi). \quad (31)$$

The energy shift $\delta_\Lambda(\bar{E}_x)$ can be separated into two components of the V_0 and S_N contributions

$$\delta_\Lambda(\bar{E}_x(I^\pi)) = \delta_{\Lambda,0}(\bar{E}_x(I^\pi)) + \delta_{\Lambda,S_N}(\bar{E}_x(I^\pi)). \quad (32)$$

In the calculation without the core polarization, the first and second components are given by energy differences in $\varepsilon_{\Lambda,0}$ and S_N contributions, respectively, between the ground and excited states as

$$\delta_{\Lambda,0}(\bar{E}_x) = \varepsilon_{\Lambda,0}(\rho_N^{I^\pi}) - \varepsilon_{\Lambda,0}(\rho_N^{\text{gs}}), \quad (33)$$

$$\delta_{\Lambda,S_N}(\bar{E}_x) = \langle V_{S_N} \rangle_{\Lambda Z}(I^\pi) - \langle V_{S_N} \rangle_{\Lambda Z}(\text{gs}). \quad (34)$$

3. spin-doublet splitting energy

The splitting energy between spin-doublet $J^\pi_>$ and $J^\pi_<$ states is given as

$$E_{\Lambda Z}(J^\pi_>) - E_{\Lambda Z}(J^\pi_<). \quad (35)$$

Here the splitting energy is defined by the energy of the $J^\pi_>$ state measured from the $J^\pi_<$ state, and a negative splitting energy means the reverse ordering case $E_{\Lambda Z}(J^\pi_>) < E_{\Lambda Z}(J^\pi_<)$. In the present perturbative treatment, the splitting energy is sum of Δ_σ , S_Λ , and T contributions,

$$\langle \Psi_{\Lambda Z}(J^\pi_>) | V_{\sigma,S_\Lambda,T} | \Psi_{\Lambda Z}(J^\pi_>) \rangle - \langle \Psi_{\Lambda Z}(J^\pi_<) | V_{\sigma,S_\Lambda,T} | \Psi_{\Lambda Z}(J^\pi_<) \rangle.$$

III. EFFECTIVE INTERACTIONS

A. Effective NN interactions

As for the effective NN interactions, the finite-range NN interactions of the Volkov central and G3RS spin-orbit forces [66, 67] are adopted. These interactions are widely used in structure studies of p -shell nuclei.

TABLE I: Parameter sets of the Volkov+G3RS NN interactions and the \bar{k}_F parameters of the ESC08a ΛNG interaction in the CL, AMD, and AMD' calculations with the hybrid k_F treatment.

set	NN central Volkov No.2		NN spin-orbit G3RS [MeV]	
NN-a	$m = 0.60, b = h = 0.125$		$u_1 = -u_2 = 1600$	
NN-a'	$m = 0.60, b = h = 0.06$		$u_1 = -u_2 = 1300$	
NN-b	$m = 0.57, b = h = 0.125$		$u_1 = -u_2 = 1200$	
NN-c	$m = 0.62, b = h = 0.125$		$u_1 = -u_2 = 820$	

${}^A_\Lambda Z$	CL		AMD		AMD'	
	set	\bar{k}_F	set	\bar{k}_F	set	\bar{k}_F
${}^7_\Lambda \text{Li}$	NN-b	0.93	NN-b	0.96		
${}^8_\Lambda \text{Li}$	NN-b	0.91	NN-b	0.96		
${}^9_\Lambda \text{Be}$	NN-a	0.90	NN-a	0.96	NN-a'	0.95
${}^{10}_\Lambda \text{Be}$	NN-a	0.95	NN-a	0.97	NN-a'	0.98
${}^{10}_\Lambda \text{B}$	NN-a	0.94	NN-a	0.96	NN-a'	0.97
${}^{11}_\Lambda \text{Be}$	NN-a	1.04	NN-a	1.10	NN-a'	1.05
${}^{11}_\Lambda \text{B}$	NN-a	1.03	NN-a	1.06	NN-a'	1.06
${}^{12}_\Lambda \text{B}$	NN-a	1.07	NN-a	1.12	NN-a'	1.11
${}^{12}_\Lambda \text{C}$	NN-a	1.06	NN-a	1.12	NN-a'	1.10
${}^{13}_\Lambda \text{C}$	NN-a	1.11	NN-a	1.18	NN-a'	1.15
${}^{16}_\Lambda \text{O}$	NN-a	1.14	NN-a	1.21	NN-c	1.20
${}^{19}_\Lambda \text{F}$	NN-c	1.18				

These effective NN interactions have adjustable parameters, which are usually tuned A_N - and model-dependently. The interaction parameters used in the present calculation are summarized in Table I. The default parameter sets are the same as those used for the cluster model calculations in the previous works [55, 58]. They are $w = 0.40$, $m = 0.60$, and $b = h = 0.125$ of the Volkov No.2 and $u_1 = -u_2 = 1600$ MeV of the G3RS for Be, B, C, and O, and $w = 0.43$, $m = 0.57$, $b = h = 0.125$, and $u_1 = -u_2 = 1200$ MeV for ${}^6\text{Li}$ and ${}^7\text{Li}$. In this paper, the former and the latter sets are called NN-a and NN-b, respectively. For ${}^{19}_\Lambda \text{F}$, the set (labeled by NN-c) of $w = 0.38$, $m = 0.62$, $b = h = 0.125$, and $u_1 = -u_2 = 820$ MeV is used. The NN-c was tuned so as to describe spectra in ${}^{17}\text{O}$ and ${}^{18}\text{F}$ with the ${}^{16}\text{O}+n$ and ${}^{16}\text{O}+p+n$ cluster model calculations [62]. The CL calculation with these default parameters of the NN interactions globally describes low-lying energy spectra in core nuclei. However, the AMD calculation with the default parameters some-

times fails to reproduce the experimental energy spectra in such nuclei as ^{10}B and ^{15}O . Instead of the NN-a, we also use an alternative set (NN-a') of modified parameters $w = 0.40$, $m = 0.60$, $b = h = 0.06$, and $u_1 = -u_2 = 1300$ MeV, which have been used in the AMD calculation of ^{10}B [54]. For the AMD calculation of ^{15}O , we try the NN-c. In most cases, the modifications of NN interaction parameters give only minor changes of nuclear structures except for energy spectra. We use the label AMD for the AMD calculation with the default parameters of the NN interactions, and the label AMD' for the AMD calculation with the set NN-a' (for ^{16}O , the label AMD' for the calculation with the set NN-c).

The parameter sets of effective NN interactions are summarized in Table I.

B. Λ - N interactions

We use the ΛNG interactions, which are derived with the G -matrix theory from the the Nijmegen extended-soft-core (ESC) model. The ΛNG interactions used here are even and odd central, triplet-odd spin-orbit, and triplet-odd tensor interactions as

$$V_{\Lambda N} = V_0 + V_\sigma + V_{S_\Lambda} + V_{S_N} + V_T, \quad (36)$$

$$V_0 = v_0^e(r)\hat{P}(E) + v_0^o(r)\hat{P}(O) \quad (37)$$

$$V_\sigma = \left[v_\sigma^e(r)\hat{P}(E) + v_\sigma^o(r)\hat{P}(O) \right] (\boldsymbol{\sigma}_\Lambda \cdot \boldsymbol{\sigma}_N) \quad (38)$$

$$V_{S_\Lambda} = v_{S_\Lambda}^o(r)\hat{P}(O)(\mathbf{l} \cdot \mathbf{s}_\Lambda) \quad (39)$$

$$V_{S_N} = v_{S_N}^o(r)\hat{P}(O)(\mathbf{l} \cdot \mathbf{s}_N) \quad (40)$$

$$V_T = v_T^o(r)\hat{P}(O)S_{12} \quad (41)$$

$$\hat{P}(E) = \frac{1 + P_r}{2} \quad (42)$$

$$\hat{P}(O) = \frac{1 - P_r}{2}. \quad (43)$$

For simplicity, the Λ - N relative momentum \mathbf{p} in the $\mathbf{l} = \mathbf{r} \times \mathbf{p}$ term of the spin-orbit interactions V_{S_Λ} and V_{S_N} is approximated to be $\mathbf{p} = (\mathbf{p}_N - \mathbf{p}_\Lambda)/2$ corresponding to the equal mass ($m_N = m_\Lambda$) approximation.

We start from the ESC08a version of the ΛNG interactions [45–47], and then consider tuning of its spin-dependent terms as described in later. In Ref. [47], the original ESC08a ΛNG interaction is given by three-range Gaussian local potentials. $v_{0,\sigma}^{e,o}(r)$ for the central interactions V_0 and V_σ are written as

$$v_{0,\sigma}^{e,o}(k_F, r) = \sum_{i=1}^3 \sum_{n=0}^2 c_{0,\sigma}^{e,o}(n, i) k_F^n \exp \left[- \left(\frac{r}{\beta_i} \right)^2 \right] \quad (44)$$

$$c_0^e(n, i) = c_{n,i}^{1E} + c_{n,i}^{3E}, \quad (45)$$

$$c_0^o(n, i) = c_{n,i}^{1O} + c_{n,i}^{3O}, \quad (46)$$

$$c_\sigma^e(n, i) = c_{n,i}^{3E} - 3c_{n,i}^{1E}, \quad (47)$$

$$c_\sigma^o(n, i) = c_{n,i}^{3O} - 3c_{n,i}^{1O}, \quad (48)$$

with the Gaussian range parameters $\beta_1 = 0.5$ fm, $\beta_2 = 0.9$ fm, and $\beta_3 = 2.0$ fm. The density dependence is taken into account by the k_F parameter. The values of $c_{n,i}^{1E}$, $c_{n,i}^{3E}$, $c_{n,i}^{1O}$, and $c_{n,i}^{3O}$ for the ESC08a are listed in Table II of Ref. [47].

TABLE II: Parameters of triplet-odd Λ -spin spin-orbit (V_{S_Λ}) and tensor (V_T) terms in the ESC08a ΛNG interaction at $k_F = 1.0$ fm $^{-1}$ from Ref. [47].

	$i = 1$	$i = 2$	$i = 3$
V_{S_Λ}			
β_i [fm]	0.4	0.8	1.2
$c_{S_\Lambda}^o$ [MeV]	2772	-106.6	-0.864
$c_{S_N}^o$ [MeV]	-684	-129.8	-4.538
V_T			
β_i [fm]	0.5	0.9	2
c_T^o [MeV]	10.37	0.0181	0.017

For the spin-orbit and tensor interactions, we use the density-independent interactions fixed at $k_F = 1.0$ fm $^{-1}$ as

$$v_{S_\Lambda, S_N}^o(r) = \sum_{i=1}^3 c_{S_\Lambda, S_N}^o(i) \exp \left[- \left(\frac{r}{\beta_i} \right)^2 \right], \quad (49)$$

$$v_T^o(r) = \sum_{i=1}^3 c_T^o(i) r^2 \exp \left[- \left(\frac{r}{\beta_i} \right)^2 \right]. \quad (50)$$

The values of range and strength parameters taken from Ref. [47] are listed in Table II.

For the k_F parameter in the central interactions, there are a couple of treatments. One is the density-dependent (DD) k_F treatment called ‘‘averaged density approximation (ADA)’’, and another is the density-independent (DI) k_F treatment with a fixed k_F value. The ΛNG interactions generally have density dependence reflecting nuclear medium effects, which are taken into account in the G -matrix theory. ESC08 versions of the ΛNG interactions was originally designed as density-dependent interactions to globally reproduce the Λ binding energies of $^A_\Lambda Z$ in a wide mass number region [42, 43, 47], whereas the DI k_F treatment has been often used in studies of energy spectra of p -shell hypernuclei. In the previous works [55, 58], applicability of the DD and DI k_F treatments for description of p -shell $^A_\Lambda Z$ energy spectra has been tested focusing on excitation energy shifts by Λ particle. The DD k_F treatment is found to be not suitable to describe the observed excitation energy shifts in $^A_\Lambda Z$. The DI k_F treatment can describe a trend of the excitation energy shifts but tends to overestimate the observed values. It suggests that a moderate density-dependence weaker than the DD k_F treatment is favored, and therefore the intermediate version (hybrid k_F treatment) between DD and DI has been proposed as an alternative

k_F treatment in Ref. [58]. In the present calculation, we adopt the hybrid k_F treatment described as follows.

In the DD k_F treatment (ADA), the k_F is taken to be $k_F = \langle k_F \rangle_\Lambda$, where $\langle k_F \rangle_\Lambda$ is the averaged Fermi momentum for the Λ distribution as

$$\langle k_F \rangle_\Lambda = \left[\frac{3\pi^2}{2} \langle \rho_N \rangle_\Lambda \right]^{1/3}. \quad (51)$$

In the hybrid k_F treatment, the average of the DD and DI interactions are used. Namely, the k_F parameter is chosen to be

$$k_F^n = (1 - e)\bar{k}_F^n + e\langle k_F \rangle_\Lambda^n, \quad (52)$$

with a weight factor $e = 0.5$. Here \bar{k}_F is the fixed input parameter. In the DD and hybrid k_F treatments, $\langle k_F \rangle_\Lambda$ is self-consistently determined for each state in the Λ -nucleus potential model. In the hybrid k_F treatment, the input parameter \bar{k}_F is chosen for each system and taken to be the mean value of $\langle k_F \rangle_\Lambda$ determined by the DD k_F treatment for the ground and excited states of the system. The used values of the input parameter \bar{k}_F in the hybrid k_F treatment are shown in Table I.

IV. PROPERTIES OF CORE NUCLEI ^{A-1}Z

In order to investigate energy spectra in $^A_\Lambda Z$, it is important that the structure models properly reproduce the structure properties such as energy spectra and radii of core nuclear states (^{A-1}Z) without a Λ . In particular, nuclear spin properties of core nuclei ^{A-1}Z are essential to discuss spin-dependent contributions of the ΛN interactions in $^A_\Lambda Z$. In this section, we show the calculated result for ^{A-1}Z . In addition to energy spectra of ^{A-1}Z , a particular attention is paid on spin configurations, which are directly reflected in spin-doublet splittings in $^A_\Lambda Z$.

A. Energies and radii of core nuclei ^{A-1}Z

The excitation energies calculated with the CL, AMD, AMD' and experimental values are summarized in Table III. The calculated energy spectra depend on the adopted NN interactions as well as the structure models. The CL result reasonably describes the low-lying energy spectra of p -shell nuclei. The AMD generally gives similar results to the CL, but there are some exceptions. For example, excitation energies of $^{10}\text{B}(1^+)$ and $^{15}\text{O}(3/2^-)$ states are much overshoot by the AMD calculation. The excitation energies of these states strongly depend on the strength of the NN spin-orbit interactions. The overshooting is improved in the AMD' calculation because of the weaker NN spin-orbit interactions in the NN-a' and NN-c than that in the NN-a.

Table IV shows the comparison of root-mean-square (rms) radii (R_p) of proton distribution obtained by the CL and AMD calculations as well as the experimental

values reduced from rms charge radii. The AMD calculation generally gives smaller R_p values than the CL calculation because the dynamical inter-cluster motion is not sufficiently taken into account in the present AMD. On the other hand, the CL model tends to give larger R_p than the AMD because the cluster breaking is not taken into account in the model. This is the major reason why we adopt the two typical nuclear models, CL and AMD, in this paper. The experimental values are found to be in between theoretical values of two calculations.

B. Spin configurations and magnetic moments of core nuclei ^{A-1}Z

Spin configurations are not so sensitive to choice of NN interactions as the energy spectra except for $p_{3/2}$ -shell closed nuclei such as ^{10}Be , ^{11}B , ^{11}C , and ^{12}C .

In $^A_\Lambda Z$ with odd-odd and even-odd (odd-even) core nuclei, the spin-doublet splitting sensitively reflects the z component S_z of the total nuclear intrinsic-spin \mathbf{S} through the $\boldsymbol{\sigma}_\Lambda \cdot \boldsymbol{\sigma}_N$ term in the Δ_σ contribution. It is able to check reliability of structure models for spin properties in comparison of μ moments in ^{A-1}Z between theory and experiment. The AMD and AMD' results for μ moments and nuclear intrinsic-spin and orbital angular momentum in nuclear states (^{A-1}Z) are shown in Table III together with the experimental μ moments. The calculation reasonably reproduces the experimental μ moments indicating that spin configurations of core nuclei are reasonably described with the AMD model.

In $Z = N$ odd-odd nuclei, ^6Li , ^{10}B , and ^{18}F , $I^\pi = 1^+$ and $I^\pi = 3^+$ states are dominantly described by pn pairs in $L = I - 1$ states with the intrinsic spin $S = 1$, which is approximately aligned to the total nuclear spin (I) as indicated by $\langle S_z \rangle \approx 1$. In particular, in ^6Li and ^{18}F states, $\alpha + pn$ and $^{16}\text{O} + pn$ structures are formed, respectively, and μ moments of 1^+ , 3^+ , and 5^+ states are close to the values $\mu = 0.88$, 1.88 and $2.88 \mu_N$ for the ideal $S = 1$ pn pairs in the $L = 0$, 2 , and 4 states, respectively.

In even-odd and odd-even nuclei, a valence nucleon spin $s = 1/2$ tends to align to the total nuclear spin in $I^\pi = 3/2^-$ states, but the alignment is not necessarily perfect because of significant configuration mixing as seen in deviation from $S_z = 0.5$. In $I^\pi = 1/2^-$ states, S_z is roughly equal to $s_z = -1/6$ for the $p_{1/2}$ single-particle contribution, but non-negligible configuration mixing is contained as indicated by the μ moments slightly deviating from the Schmidt values ($\mu_{\text{Schmidt}} = -0.79 \mu_N$ for a proton and $0.64 \mu_N$ for a neutron) except for $^{15}\text{O}(1/2^-)$. In $^{15}\text{O}(1/2^-)$, the spin configuration is understood by almost the pure $p_{1/2}$ hole configuration.

In $Z = N = 2n$ nuclei, $n\alpha$ -cluster structures are favored. Particularly, the $^8\text{Be}(0^+, 2^+)$ states have remarkable 2α -cluster structures and almost pure $S = 0$ components. On the other hand, the $^{12}\text{C}(0^+)$ and $^{12}\text{C}(2^+)$ states contain significant $S \neq 0$ components because of

3α -cluster breaking. The $S \neq 0$ mixing is sensitive to the NN spin-orbit interactions especially in $^{12}\text{C}(0^+)$. The mixing in $^{12}\text{C}(0^+)$ is less in the AMD' than the AMD because of the weaker NN spin-orbit interaction. Compared with $^{12}\text{C}(0^+)$, the $S \neq 0$ component in $^{12}\text{C}(2^+)$ is relatively small and not so sensitive to the NN interactions, but it still gives non-negligible Δ_σ and T contributions to the spin-doublet splitting in ^{13}C spectra as discussed later.

V. RESULTS OF Λ HYPERNUCLEI: $^A_\Lambda Z$

A. Averaged structure properties of $^A_\Lambda Z$ states obtained with spin-independent ΛN interactions

In this subsection, we show calculated results of averaged structure properties of $^A_\Lambda Z$ states obtained with the leading part V_0 (spin-independent) of the ΛN interactions without the perturbative part V_1 .

Table V shows the calculated results of the Λ binding energies ($\bar{B}_{\Lambda,0}$), rms radii of the Λ and nuclear distributions (r_Λ and R_N), and averaged Fermi momentum ($\langle k_F \rangle_\Lambda$) obtained with the CL and AMD. The experimental data of the Λ binding energy (B_Λ) and spin-averaged one (\bar{B}_Λ) are shown for comparison. The systematics of the observed Λ binding energies is reasonably described by the leading part V_0 of ECS08a(Hyb) interaction. The model dependence of $\bar{B}_{\Lambda,0}$ between the CL and AMD is not so strong. Quantitatively, the Λ binding is slightly deeper in the AMD than the CL except for $^{12}\text{B}(3/2^-_{\text{gs}})$, $^{12}\text{C}(3/2^-_{\text{gs}})$, and $^{13}\text{C}(0^+)$, because the AMD tends to give smaller nuclear radii R_N , i.e., the higher nuclear density contributing the deeper Λ -core potential.

The Λ distribution size (r_Λ) is larger than the nuclear matter distribution size (R_N) in light-mass $^A_\Lambda Z$ because of small Λ binding energies. With increase of the mass number A , r_Λ becomes gradually small as the Λ binding becomes deep. The nuclear matter radii R_N increase with the increase of A , and in heavy-mass p -shell $^A_\Lambda Z$ it is eventually as large as r_Λ . Densities of Λ and nuclear distributions are shown in Fig. 1. The mass number dependence of the Λ distribution is very mild compared with that of nuclear matter distributions.

B. Tuning of spin-dependence of ΛN interactions

The Δ_σ term of the ESC08(a,b) ΛNG interaction is known to be inappropriate to describe the observed spin-doublet splitting energies. For example, the ESC08a gives the reverse ordering of the $J_>$ and $J_<$ states in ^{12}C and ^{11}B for the ground state core nuclei inconsistently with the experimental observation as pointed out in Ref. [47]. Other spin-dependent terms of the ESC08a ΛNG interaction have not been well tested yet. In the present work, we phenomenologically tune the spin-dependent terms of the ESC08a ΛNG interaction by

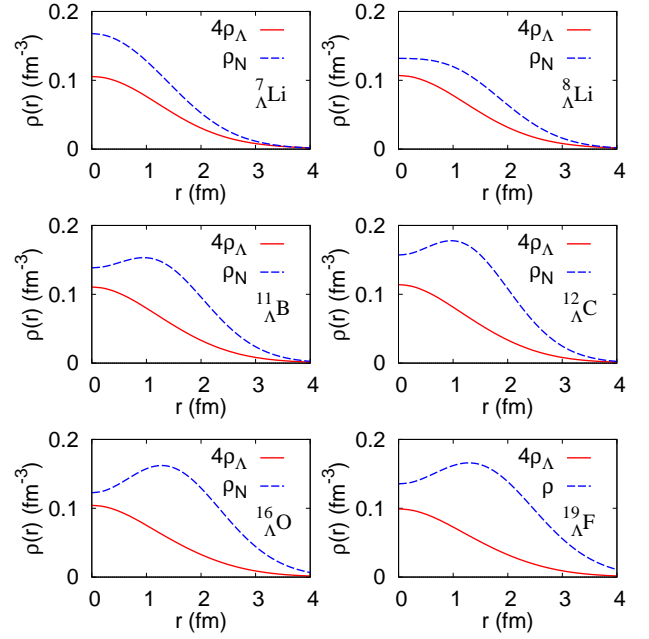


FIG. 1: (color online) Distributions of the Λ ($\rho_\Lambda(r)$) and nuclear matter ($\rho_N(r)$) densities in $^7_\Lambda\text{Li}$, $^8_\Lambda\text{Li}$, $^{11}_\Lambda\text{B}$, $^{12}_\Lambda\text{C}$, $^{16}_\Lambda\text{O}$, and $^{19}_\Lambda\text{F}$ obtained with the CL calculation using the spin-independent ΛN interactions (V_0).

modifying the original strength parameters to describe energy spectra in p -shell Λ hypernuclei as follows.

- For the spin-independent term V_0 , the original parameters are used.
- The Δ_σ term (V_σ) is adjusted so as to globally describe the $3/2^- - 1/2^-$ and $7/2^- - 5/2^-$ splittings in $^7_\Lambda\text{Li}$ and $^{11}_\Lambda\text{B}$, which are dominantly contributed by the Δ_σ term because of the total nuclear intrinsic-spin $S = 1$ component. The even and odd parts of V_σ are multiplied by factors of 2 and 0.3, respectively.
- For the T term (V_T), the observed value of the $1^- - 0^-$ splitting in $^{16}_\Lambda\text{O}$ is used as an input parameter for tuning. In the $1^- - 0^-$ splitting, the T contribution is relatively large compared with other systems and cancels the Δ_σ contribution. The strength of V_T is multiplied by a factor of 6 to fit the small $1^- - 0^-$ splitting observed in $^{16}_\Lambda\text{O}$.
- The spin-orbit terms (V_{S_Λ} and V_{S_N}) are not modified. These contributions in splitting energies are generally small and it is difficult to definitely determine these terms without ambiguity from existing data, and therefore, these terms are tentatively left as they are. However, it is likely that a larger V_{S_Λ} term with a factor of ~ 2 than the original one is favored to reproduce the $5/2^+ - 3/2^+$ splitting in ^9Be .

As a result, above modifications $v(r) \rightarrow \tilde{v}(r)$ are expressed as

$$\tilde{v}_0^{e,o}(r) = v_0^{e,o}(r), \quad (53)$$

$$\tilde{v}_\sigma^{e,o}(r) = f_\sigma^{e,o} v_\sigma^{e,o}(r), \quad (54)$$

$$\tilde{v}_{S_\Lambda}^o(r) = f_{S_\Lambda} v_{S_\Lambda}^o(r), \quad (55)$$

$$\tilde{v}_{S_N}^o(r) = f_{S_N} v_{S_N}^o(r), \quad (56)$$

$$\tilde{v}_T^o(r) = f_T v_T^o(r), \quad (57)$$

with $f_\sigma^e = 2$, $f_\sigma^o = 0.3$, $f_{S_\Lambda} = f_{S_N} = 1$, and $f_T = 6$. We call the ESC08a $\Lambda N G$ interaction with thus modified spin dependence (msd) “ESC08a-msd”. In the following sections, we first show the crucial problem of the original spin-dependent interactions of ESC08a in reproducing the experimental spin-doublet splitting energies and how the results are improved by the modified interactions, ESC08a-msd. Then, we discuss the details of energy spectra in ${}^A_\Lambda Z$ based on the calculations with the ESC08a-msd, which we use as the default ΛN interactions unless otherwise specified.

C. Spin-doublet splitting energies: general features

The spin-doublet splitting energies and respective contributions calculated with the original ESC08a and ESC08a-msd interactions are shown in Table VI together with the experimental data. Significant splittings have been experimentally observed for such core nuclear states as ${}^{A-1}Z(1_1^+)$ and ${}^{A-1}Z(3_1^+)$ in $Z = N$ odd-odd nuclei and ${}^{A-1}Z(3/2_{gs}^-)$ and ${}^{A-1}Z(5/2_1^-)$ in even-odd and odd-even core nuclei. However, the original ESC08a $\Lambda N G$ interaction gives opposite-sign splitting energies, namely, the reverse ordering of the spin-doublet partners because opposite-sign contributions from the odd term of V_σ dominate the Δ_σ contributions. It is a crucial problem of the spin dependence of the original ESC08a as pointed out in Ref. [47]. In contrast, the spin-doublet splitting energies are reasonably reproduced by the ESC08a-msd with the modified spin-dependence of the ΛN interactions. The significant splittings observed for ${}^{A-1}Z(1_1^+)$ and ${}^{A-1}Z(3_1^+)$ of $Z = N$ odd-odd nuclei, and ${}^{A-1}Z(3/2_{gs}^-)$ and ${}^{A-1}Z(5/2_1^-)$ of even-odd and odd-even core nuclei are described by the dominant Δ_σ contributions in the present AMD calculation with the ESC08a-msd. T contributions are usually small compared with dominant Δ_σ contributions except for core ${}^{A-1}Z(1/2^-)$ states in odd-even and even-odd nuclei, in which the T and Δ_σ contributions are comparable order and almost cancel with each other. The S_Λ term gives minor contributions in general.

The present result of splitting energies is compared with SM calculations in Table VII. Each contribution is also compared with that of the SM calculation by Millener *et al.* [28]. In general, the Δ_σ , S_Λ , and T contributions obtained in the present calculation are similar to those of the Millener’s SM calculation. This

is a natural consequence because, in both calculations, spin-dependent contributions are phenomenologically adjusted to fit the observed splitting energies in p -shell ${}^A_\Lambda Z$.

The present AMD calculation with the ESC08a-msd interaction, reasonably describes the global feature of observed data of spin-doublet splittings in p -shell ${}^A_\Lambda Z$ though agreements with the experimental value are not so precise as the Millener’s SM calculation [28]. It should be commented that, in the Millener’s SM calculation, the spin-dependent ΛN interaction parameters are independently adjusted to the light- and heavy-mass p -shell regions, whereas in the present calculation the mass-number independent ΛN interactions are used.

Let us discuss the NN interaction dependence of splitting energies. In Table VIII, we compare the AMD result (the stronger NN spin-orbit interaction) and the AMD’ result (the weaker NN spin-orbit interaction). The difference of the NN spin-orbit interaction causes slight difference in the nuclear intrinsic-spin configurations. Generally, weaker NN spin-orbit interaction enhances the LS -coupling component and reduces the jj -coupling component (the cluster breaking). However, in most cases, the NN interaction difference between the AMD’ and AMD gives only minor difference in the splittings because nuclear intrinsic-spin configurations are not so sensitive to the NN interactions as shown in Table III.

D. Spin-doublet splitting energies: characteristics in cases of odd-odd, even-odd(odd-even), and even-even core nuclei

We here discuss characteristics of splitting energies in cases of odd-odd, even-odd(odd-even), and even-even core nuclei based on the AMD results with the ESC08a-msd in Table VI and the comparison with the SM calculations in Table VII.

1. Case of $Z = N$ odd-odd core nuclei: $3/2^+ - 1/2^+$ and $7/2^+ - 5/2^+$ splittings in ${}^7_\Lambda \text{Li}$, ${}^{11}_\Lambda \text{B}$, and ${}^{19}_\Lambda \text{F}$

In the case of ${}^A_\Lambda Z$ with $Z = N$ odd-odd core nuclei, one of the characteristics of $T = 0$ states is remarkably large splitting energies because of the dominant nuclear intrinsic-spin $S = 1$ component contributed by two valence nucleons, a proton and a neutron. As shown in Table III, the core nuclear states, $I^\pi = 1^+$, 3^+ , and 5^+ have $S = 1$ and $T = 0$ pn pairs in the $L = 0, 2$, and 4 waves as dominant components, respectively. The aligned nuclear intrinsic-spin $S_z \approx 1$ provides the significant Δ_σ contribution in the splitting.

The mass number dependence of Δ_σ comes from the difference in spatial overlap between valence nucleon and Λ orbits. In ${}^{19}_\Lambda \text{F}$, the $0s$ -orbit Λ has a smaller overlap with the sd -orbit proton and neutron than in ${}^7_\Lambda \text{Li}$ and ${}^{11}_\Lambda \text{B}$ having the valence proton and neutron in the p -shell. In each ${}^A_\Lambda Z$ system, higher J states tend to have smaller

splittings because of negative contributions from the T and S_Λ terms.

The splittings in ${}^7_\Lambda\text{Li}$ have been investigated in details by the OCM (semi-microscopic) cluster model calculation with the NSC97f $\Lambda N G$ interactions [14]. In the OCM calculations with the NSC97f, the Δ_σ contribution in the $3/2^+-1/2^+(7/2^+-5/2^+)$ splitting is $\Delta_\sigma = 0.71(0.54)$ MeV with even and odd contributions, $\Delta_\sigma^e = 1.10(1.04)$ MeV and $\Delta_\sigma^o = -0.39(-0.50)$ MeV, respectively. In the present AMD with the ESC08a-msd, it is $\Delta_\sigma = 0.52(0.47)$ MeV with $\Delta_\sigma^e = 0.75(0.72)$ MeV and $\Delta_\sigma^o = -0.22(-0.25)$ MeV. The present result is qualitatively consistent with but quantitatively slightly smaller than the OCM calculation and also slightly underestimates the experimental data. For more precise reproduction of the splittings in ${}^7_\Lambda\text{Li}$, higher order effects beyond the s -wave Λ approximation should be taken into account.

For ${}^{19}_\Lambda\text{F}$, the AMD calculation gives the $3/2^+-1/2^+$ splitting of 0.249 MeV, which reasonably agrees with the experimental value 0.315 MeV recently observed by the γ -ray measurement [4]. For the $7/2^+-5/2^+$ and $11/2^+-9/2^+$ splittings in ${}^{19}_\Lambda\text{F}$, the present calculation predicts smaller splittings than the $3/2^+-1/2^+$ splitting because of the cancellation of the dominant Δ_σ contribution by opposite-sign T and S_Λ contributions. Our result is consistent with Millener's SM prediction but seems appreciably different from the prediction estimated with NSC97f G -matrix interaction by Umeya et al. [90].

2. Case of even-odd and odd-even core nuclei: splittings in ${}^8_\Lambda\text{Li}$, ${}^{10}_\Lambda\text{Be}$, ${}^{12}_\Lambda\text{B}$, ${}^{12}_\Lambda\text{C}$, ${}^{16}_\Lambda\text{O}$

In ${}^A_\Lambda Z$ with even-odd and odd-even core nuclei, the 2^--1^- and 3^--2^- splittings for core $I^\pi = 3/2^-$ and $5/2^-$ states are moderate. They are mainly contributed by the valence nucleon spin $S = 1/2$ in the p -shell through the Δ_σ term. The exception is the splitting for the core ${}^7\text{Li}(5/2^-)$ state, which is described by the t cluster orbiting in the $L = 3$ wave around the α cluster. In the $I^\pi = 5/2^-$ state, the t -cluster intrinsic-spin $S = 1/2$ is coupling with the $L = 3$ with the anti-parallel orientation, and gives a negative contribution to the splitting. As a result, the ordering of the 3^- and 2^- states are reverse in ${}^8_\Lambda\text{Li}$. As for the splittings in ${}^{10}_\Lambda\text{Be}$, our result is similar to the SM predictions in Refs. [28, 88]. On the other hand, the four-body OCM cluster model calculation [16] gives quite small values in ${}^{10}_\Lambda\text{Be}$ as 0.08 MeV and 0.05 MeV for the 2^--1^- and 3^--2^- splittings, which are inconsistent with our result and SM predictions.

In ${}^8_\Lambda\text{Li}$, ${}^{10}_\Lambda\text{Be}$, ${}^{12}_\Lambda\text{B}$, ${}^{12}_\Lambda\text{C}$, and ${}^{16}_\Lambda\text{O}$, the 1^--0^- splittings for core $I^\pi = 1/2^-$ states are remarkably small because significant negative contributions of the tensor (T) term cancels the Δ_σ contribution. As pointed out by Millener, this cancellation is essential to describe the small 1^--0^- splitting observed in ${}^{16}_\Lambda\text{O}$. Indeed, the Millener's SM calculation predicts the small 1^--0^- splittings in ${}^8_\Lambda\text{Li}$, ${}^{10}_\Lambda\text{Be}$, ${}^{12}_\Lambda\text{B}$, and ${}^{12}_\Lambda\text{C}$, and our result is consistent with

it. The 1^--0^- splitting is experimentally known only for ${}^{16}_\Lambda\text{O}$ but not for other ${}^A_\Lambda Z$. In both the present and Millener's SM calculations, the value for ${}^{16}_\Lambda\text{O}$ is used as an input data in phenomenological tuning of the spin-dependent ΛN interactions. In order to check validity of the tensor term of the spin-dependent ΛN interactions, experimental data for other systems are requested.

Let us turn to the 2^--1^- splitting in ${}^{12}_\Lambda\text{B}({}^{12}_\Lambda\text{C})$ for the excited core, $I^\pi = 3/2^-$ state. The nuclear intrinsic-spin and orbital angular momentum coupling in the ${}^{11}\text{B}(3/2^-)({}^{11}\text{C}(3/2^-))$ state is quite different from that in the ground state, $I^\pi = 3/2^-$ (cf. Table III). The $I^\pi = 3/2^-$ state dominantly contains the nuclear orbital angular momentum $L = 2$ excitation coupled with a p -orbit valence nucleon as $[p_{3/2,1/2} \otimes L = 2]_{J=3/2}$ as indicated by the large $\langle L^2 \rangle$ in Table III. Because of the significant coupling with $L = 2$, the nuclear intrinsic-spin of the $p_{3/2}$ valence nucleon is not aligned to the I direction, and therefore, gives a relatively small Δ_σ contribution to the 2^--1^- splitting in ${}^{12}_\Lambda\text{B}({}^{12}_\Lambda\text{C})$. On the other hand, the T and S_Λ terms give negative contributions. As a result, the AMD (AMD') calculation give the negative values $-0.045(-0.071)$ and $-0.047(-0.073)$ MeV of the total 2^--1^- splittings namely, the reverse ordering for the core states ${}^{11}\text{B}(3/2^-)$ and ${}^{11}\text{C}(3/2^-)$, respectively (cf. Tables VI and VIII). The experimental value of this splitting has not been determined yet. The 1^- state at 6.050 MeV in ${}^{12}_\Lambda\text{C}$ has been determined by the γ -ray measurement [87], whereas the 1^- and 2^- states in ${}^{12}_\Lambda\text{B}$ are not separated but both are included in the peak observed at 5.92 ± 0.13 MeV in the $(e, e'K^+)$ reaction experiment [77]. Provided that the Coulomb shift between mirror states in ${}^{12}_\Lambda\text{C}$ - ${}^{12}_\Lambda\text{B}$ is the same as that in ${}^{11}\text{C}$ - ${}^{11}\text{B}$, the 2^--1^- splitting for $I^\pi = 3/2^-$ is estimated to be -0.215 MeV. The reverse ordering is consistent with the AMD prediction, but quantitatively the agreement is not so good. The negative splitting (reverse ordering) is also predicted by the SM calculation (theoretical value is -0.122 MeV) [89]. More detailed experimental spectra are demanded to determine the splitting energy.

3. Case of even-even $Z = N$ core nuclei: $5/2^+-3/2^+$ splitting in ${}^9_\Lambda\text{Be}$ and ${}^{13}_\Lambda\text{C}$

For ${}^9_\Lambda\text{Be}$ and ${}^{13}_\Lambda\text{C}$, we discuss spin-dependent contributions in the $5/2^+-3/2^+$ splittings for the excited core states, ${}^8\text{Be}(2^+)$ and ${}^{12}\text{C}(2^+)$. The splittings are generally small because $n\alpha$ -cluster structures are favored and the nuclear intrinsic-spin is almost saturated. In ${}^9_\Lambda\text{Be}$, since the core state ${}^8\text{Be}(2^+)$ has the ideal 2α -cluster structure with the relatively $L = 2$ wave, the Δ_σ and T contributions almost vanish and only the S_Λ term contributes to the splitting. It means that the $5/2^+-3/2^+$ splitting in ${}^9_\Lambda\text{Be}$ can be a sensitive probe to test the S_Λ term of the ΛN interactions. A tiny splitting -0.023 MeV is obtained in the AMD calculation. In the present calculation, the strength of the S_Λ term is not modified. If

the strength is tuned to fit the observed value -0.043 , a slightly stronger S_Λ term by a factor of ~ 2 is favored. This modification of the S_Λ term gives only minor effects to the splittings in other systems.

In $^{13}_\Lambda\text{C}$, the core state $^{12}\text{C}(2^+)$ contains the slight $S \neq 0$ component because of 3α -cluster breaking as can be seen in non-zero expectation value $\langle S^2 \rangle \neq 0$ in Table III. The $S \neq 0$ component from the cluster breaking gives non-negligible Δ_σ and T contributions, which cancel the negative S_Λ contribution in the $5/2^+-3/2^+$ splitting (see Table VIII). Consequently, the predicted $5/2^+-3/2^+$ splitting in $^{13}_\Lambda\text{C}$ is a small positive value, 0.064 MeV in the AMD and 0.026 MeV in the AMD' result. The difference between the AMD and AMD' results originates in the nuclear spin-orbit interaction dependence of the cluster breaking in the core state. If the twice stronger S_Λ interaction adjusted to the $5/2^+-3/2^+$ splitting in $^9_\Lambda\text{Be}$ is adopted, further cancellation occurs in $^{13}_\Lambda\text{C}$.

The ΛN spin-orbit splittings in $^9_\Lambda\text{Be}$ and $^{13}_\Lambda\text{C}$ have been investigated by the 2α - and 3α -cluster OCM calculations [12]. In the OCM cluster model calculations, the nuclear intrinsic-spin completely vanishes and only the S_Λ term contributes to the $5/2^+-3/2^+$ splittings because α clusters are assumed. The cluster OCM calculations with the NSC97f predicted the negative $5/2^+-3/2^+$ splittings as -0.16 MeV in $^9_\Lambda\text{Be}$ and -0.29 MeV in $^{13}_\Lambda\text{C}$. Compared with the later observed value -0.043 MeV in $^9_\Lambda\text{Be}$, the prediction suggests that the S_Λ term of the NSC97f interaction may be too strong.

E. S_N contributions to energy spectra and B_Λ

1. Excitation energy shifts

In the present perturbative treatment of the spin-dependent part V_1 of the ΛN interactions, the S_N term gives no contribution to the spin-doublet splitting but contributes to the spin-averaged excitation energy shift $\delta_\Lambda(\bar{E}_x(I^\pi))$. The spin-averaged excitation energy shift originates in the nuclear structure difference between the ground and excited states, and is given by two contributions, the V_0 contribution ($\delta_{\Lambda,0}(\bar{E}_x)$) and the S_N contribution ($\delta_{\Lambda,S_N}(\bar{E}_x)$), as explained in Eq. (32). The V_0 contribution reflects mainly the difference in the core nuclear size, whereas the S_N contribution is sensitive to that in the nuclear intrinsic-spin and orbital angular momentum configurations.

Table IX shows the V_0 and S_N contributions in $\delta_\Lambda(\bar{E}_x)$ as well as total values obtained by AMD and CL+AMD calculations together with the experimental data. In both the calculations, the S_N contributions are calculated with the AMD except for $^{19}_\Lambda\text{F}$ as explained previously. The expectation values $\langle V_{S_N} \rangle$ calculated with the AMD are also shown in the table. In Fig. 2, the V_0 contributions and the total excitation energy shifts are shown compared with observed values of $\delta_\Lambda(\bar{E}_x)$. As shown in the table and figure, the CL calculation tends

to give larger V_0 contributions than the AMD calculation because it gives larger size difference between the ground and excited states. The S_N contributions are relatively minor in light-mass nuclei, whereas they are comparable or even larger than the V_0 contributions in heavy-mass nuclei. Both the AMD and CL+AMD calculations qualitatively describe systematic behavior of the experimental $\delta_\Lambda(\bar{E}_x)$ in p -shell $^A_\Lambda Z$. Quantitatively, the CL+AMD (AMD) calculation more or less overestimates (underestimates) the observed data in the $A \geq 11$ region.

In Figs. 2(c) and (d), we also show the CL+AMD' result of $\delta_\Lambda(\bar{E}_x)$ to see the NN spin-orbit interaction dependence. Note that the difference between the CL+AMD and CL+AMD' calculations is the difference in the S_N contribution between the AMD and AMD' calculations. In most states except for $^{12}_\Lambda\text{B}(I^\pi = 3/2^-)$ and $^{13}_\Lambda\text{C}(I^\pi = 2^+)$, difference between two calculations is rather small indicating that the dependence in the excitation energy shift is minor. However, significant difference is found in $^{12}_\Lambda\text{B}(I^\pi = 3/2^-)$ and $^{13}_\Lambda\text{C}(I^\pi = 2^+)$, in which nuclear intrinsic-spin configurations are sensitive to the NN spin-orbit interaction as seen in Table IX. In these states, the S_N contribution is smaller in the AMD' calculation because of the less cluster breaking than the AMD calculation.

Let us discuss the $^{16}_\Lambda\text{O}$ core vibration effect to the V_0 contribution in $^{16}_\Lambda\text{O}$ and $^{19}_\Lambda\text{F}$, which are taken into account in the CL calculation of $^{16}_\Lambda\text{O}$ and the CL- 4α calculation of $^{19}_\Lambda\text{F}$. For $^{19}_\Lambda\text{F}$, the CL- 4α result is compared with the CL one, and for $^{16}_\Lambda\text{O}$, the AMD result is compared with the CL+AMD one in Table IX. In both systems, the 4α vibration gives only minor effect in the total excitation energy shifts.

2. S_N contributions to binding energies \bar{B}_Λ

The S_N term of the ΛN interactions also contributes to the Λ binding energies \bar{B}_Λ . In particular, spin-orbit favored states in core nuclei gain much potential energy because the $0s$ -orbit Λ enhances the single-nucleon (mean) spin-orbit potential through the $\mathbf{l} \cdot \mathbf{s}_N$ term in V_{S_N} . Its expectation value in the ground state is nothing but the S_N contribution to the Λ binding energies as $\bar{B}_{\Lambda,S_N} = -\langle V_{S_N} \rangle$. As expected, the S_N term gives non-negligible contributions to \bar{B}_Λ for the spin-orbit favored ground states such as $^{11}_\Lambda\text{Be}(I^\pi = 0^+)$, $^{11}_\Lambda\text{B}(I^\pi = 3^+)$, $^{12}_\Lambda\text{B}(I^\pi = 3/2^-_{\text{gs}})$, $^{12}_\Lambda\text{C}(I^\pi = 3/2^-_{\text{gs}})$, and $^{13}_\Lambda\text{C}(I^\pi = 0^+)$, whereas it gives minor contributions to well clustered states in light-mass $^A_\Lambda Z$ (see Table IX). There remains ambiguity in the result because the S_N contribution depends on the NN spin-orbit interaction. For $^{11}_\Lambda\text{Be}(I^\pi = 0^+)$, $^{11}_\Lambda\text{B}(I^\pi = 3^+)$, $^{12}_\Lambda\text{B}(I^\pi = 3/2^-_{\text{gs}})$, $^{12}_\Lambda\text{C}(I^\pi = 3/2^-_{\text{gs}})$, and $^{13}_\Lambda\text{C}(I^\pi = 0^+)$, the AMD' result of $\langle V_{S_N} \rangle$ is about half of the AMD result as $\langle V_{S_N} \rangle = -0.27, -0.36, -0.38, -0.38$ and -0.30 in MeV, respectively. Another ambiguity comes from the V_{S_N} term of the ΛN interactions, which has not been checked yet in the present work.

F. Energy spectra

Energy spectra in ${}^7_\Lambda\text{Li}$, ${}^{11}_\Lambda\text{B}$, ${}^{12}_\Lambda\text{C}$, ${}^{16}_\Lambda\text{O}$, and ${}^{19}_\Lambda\text{F}$ are shown in Figs. 3 and 4. For ${}^7_\Lambda\text{Li}$ and ${}^{12}_\Lambda\text{C}$, spectra calculated with the AMD and CL+AMD are shown, and for ${}^{19}_\Lambda\text{F}$ those with the CL calculation are shown. For ${}^{11}_\Lambda\text{B}$ and ${}^{16}_\Lambda\text{O}$, the spectra obtained with the CL+AMD and AMD' are shown. In the figures, the original energy spectra in ${}^A Z$, spin-averaged energy spectra in ${}^A_\Lambda Z$, and spectra in ${}^A_\Lambda Z$ are shown in the left, middle, and right columns, respectively.

1. Energy spectra of ${}^7_\Lambda\text{Li}$ and ${}^{11}_\Lambda\text{B}$

In the spin-averaged energy spectra in ${}^7_\Lambda\text{Li}$ and ${}^{11}_\Lambda\text{B}$, the excitation energy of ${}^6\text{Li}(3^+)$ is shifted downward in ${}^7_\Lambda\text{Li}(3^+)$, whereas that of ${}^{10}\text{B}(1^+)$ is shifted upward in ${}^{11}_\Lambda\text{B}(1^+)$ because of the V_0 and S_N contributions (cf. Table IX). In the energy spectra in ${}^7_\Lambda\text{Li}$ and ${}^{11}_\Lambda\text{B}$, the significant spin-doublet splitting occurs mainly because of the Δ_σ term contributed by $S = 1$ pn pairs around the α - and 2α -cluster structures, respectively.

The present result of excitation energy shifts and spin-doublet splitting energies in ${}^7_\Lambda\text{Li}$ and ${}^{11}_\Lambda\text{B}$ are qualitatively consistent with the experimental spectra. Strictly speaking, however, the agreement with the energy spectra is not perfect. For example, the excitation energies of ${}^7_\Lambda\text{Li}(7/2^+)$ and ${}^7_\Lambda\text{Li}(5/2^+)$ are underestimated, in particular, by the CL calculation. The reason may be that the s -orbit Λ approximation is not enough for the core nucleus ${}^6\text{Li}$ having the remarkable $\alpha + d$ cluster structure, and may overestimate the energies of ${}^7_\Lambda\text{Li}(3/2^+)$ and ${}^7_\Lambda\text{Li}(1/2^+)$ for the core ${}^6\text{Li}(1^+)$ state. In order to discuss detailed energy spectra in ${}^7_\Lambda\text{Li}$, more precise calculations with microscopic three-body or four-body cluster models are needed as has been tried in Refs. [11, 14].

2. Energy spectra of ${}^{12}_\Lambda\text{C}$

Available data of energy spectra in ${}^{12}_\Lambda\text{C}$ are reasonably reproduced by the calculations. The excitation energies for ${}^{11}\text{C}(1/2^-)$, ${}^{11}\text{C}(5/2^-)$, and ${}^{11}\text{C}(3/2^-)$ are significantly raised because of the stronger binding energy between Λ and ${}^{11}\text{C}(3/2^-_{gs})$ (cf. Table V). The spin-doublet splittings for the core ${}^{11}\text{C}(3/2^-_{gs})$ and ${}^{11}\text{C}(5/2^-)$ are moderate because, as a leading order, one valence nucleon spin contributes to the splittings. The spin-doublet splittings have not been measured yet except for the 2^-_1 - 1^-_1 splitting in ${}^{12}_\Lambda\text{C}$. For the core excited state, ${}^{11}\text{C}(3/2^-)$, the negative splitting energy, i.e., the reverse ordering of the spin-doublet states is predicted. The present prediction is supported by the experimental excitation energy of the mirror 2^- state in ${}^{12}_\Lambda\text{B}$ measured by the production cross section analysis [77].

3. Energy spectra of ${}^{16}_\Lambda\text{O}$

The experimental spectra in ${}^{16}_\Lambda\text{O}$ are reproduced well by the calculations. The spin-averaged excitation energy for the core ${}^{15}\text{O}(3/2^-)$ state is shifted upward by the Λ mainly because of the S_N contribution. The V_0 contribution to the excitation energy shift is minor. The AMD' and CL+AMD results are similar indicating that the vibration effect in the ${}^{16}_\Lambda\text{O}$ core is minor because the ${}^{15}\text{O}$ structure is rather robust differently from fragile cluster structures of light-mass p -shell nuclei. The spin-doublet splittings for the core states, ${}^{15}\text{O}(1/2^-)$ and ${}^{15}\text{O}(3/2^-)$, are tiny and moderate, respectively, reflecting the nuclear spin configurations in the core nucleus.

4. Energy spectra of ${}^{19}_\Lambda\text{F}$

The recently observed 0.315 MeV and 0.895 MeV γ -rays are assigned to the $M1$ $3/2^+ \rightarrow 1/2^+$ and $E2$ $5/2^+ \rightarrow 1/2^+$ transitions, respectively [4]. The calculated value 0.25 MeV of the $3/2^+-1/2^+$ splitting is in reasonable agreement with the observed value 0.315 MeV. The $3/2^+-1/2^+$ splitting is contributed mainly by the Δ_σ term, which reflects the dominant nuclear intrinsic-spin $S = 1$ component of a pn pair in the $L = 0$ wave. For the $7/2^+$ and $5/2^+$ states, a smaller splitting 0.18 MeV than the $3/2^+-1/2^+$ splitting is predicted because of the cancellation of the Δ_σ contribution by the T and L_Λ contributions as discussed previously.

Let us discuss the detail of the excitation energy $E_x(5/2^+)$ in ${}^{19}_\Lambda\text{F}$. The experimental energy shift -0.042 MeV of ${}^{19}_\Lambda\text{F}(5/2^+)$ is reduced from the observed $E_x(5/2^+) = 0.895$ MeV in ${}^{19}_\Lambda\text{F}$ and $E_x(3^+) = 0.937$ MeV in ${}^{18}\text{F}$. The calculated energy shift is -0.03 (-0.07) MeV in the CL ($\text{CL}^{4\alpha} + \text{CL}$) calculations. The result reasonably agrees with the experimental data. In the CL calculation, the S_N and V_0 contributions are -0.05 MeV and -0.04 MeV, respectively. In addition, the spin-doublet splitting energy gives positive contribution of $+0.07$ MeV to the excitation energy shift because it causes larger energy gain in the ground ${}^{19}_\Lambda\text{F}(1/2^+)$ state than the ${}^{19}_\Lambda\text{F}(5/2^+)$ state. For more detailed discussion, the experimental measurement of the excitation energy for the spin-doublet partner ${}^{19}_\Lambda\text{F}(7/2^+)$ is highly requested.

VI. SUMMARY

Energy spectra of $0s$ -orbit Λ states in p -shell Λ hypernuclei (${}^A_\Lambda Z$) and those in ${}^{19}_\Lambda\text{F}$ were studied with the AMD+VAP and microscopic cluster model using the ΛNG interactions. The spin-dependent terms of the ESC08a ΛNG interaction were tested in comparison of the calculated energy spectra with the observed ones. A modification of the spin-dependence of the ESC08a ΛNG interaction was proposed by phenomenological tuning of

the spin-spin ($\sigma_\Lambda \cdot \sigma_N$) and tensor (S_{12}) terms to adjust available data of energy spectra in p -shell ${}^A_\Lambda Z$.

The spin-dependent contributions of the ΛN interactions to spin-doublet splittings were discussed. In the case of odd-odd, even-odd, and odd-even core nuclei, the Δ_σ contribution is usually dominant, whereas the T and S_Λ contributions are relatively minor in most cases. There are some exceptions such as $I^\pi = 1/2^-$ states in even-odd and odd-even core nuclei, in which the significant tensor contribution cancels the Δ_σ contribution. In ${}^{13}_\Lambda\text{C}$, the cluster breaking component gives non-negligible contributions to the splitting energy for the core ${}^{12}\text{C}(2^+)$ state through the Δ_σ and tensor terms of the ΛN interactions. The V_0 and S_N contributions to the excitation energy shifts were also discussed. Calculated energy spectra as well as spin-averaged energy spectra in ${}^A_\Lambda Z$ were compared with experimental data. The calculations reasonably reproduce the observed spectra in p -shell ${}^A_\Lambda Z$ and ${}^{19}_\Lambda\text{F}$.

The extensive data of p -shell ${}^A_\Lambda Z$ observed by high-resolution γ -ray measurements are useful information to obtain comprehensive understanding of the energy spectra and structures of Λ hypernuclei. Moreover, they are useful to test the effective ΛN interactions in hypernuclei. In particular, the spin-doublet splitting is good probe to check the spin-dependence of the ΛN interactions. In the present systematic investigation of energy spectra in ${}^A_\Lambda Z$, we proposed the modified spin-dependent ΛN interactions which can reasonably reproduce the observed spin-doublet splitting energies in p -shell ${}^A_\Lambda Z$. The present work may shed a light on spin-dependence of the effective ΛN interactions in p -shell ${}^A_\Lambda Z$ and enable us to predict spectra for unobserved excited states. In order to explore such systematic investigations of Λ hypernuclei in a wide mass number region, further γ -ray spectroscopic studies of Λ hypernuclei in heavier mass regions are requested.

In the present work, two models, the AMD+VAP and microscopic cluster models, were adopted. The former is useful to treat nuclear intrinsic-spin configurations in detail, whereas the latter is suitable to describe the dynamical inter-cluster motion. In order to investigate energy spectra in ${}^A_\Lambda Z$ precisely, further advanced frameworks that can describe details of intrinsic-spin configurations as well as dynamical structure change are needed. The HAMD method is one of the promising tools. The ambiguity in the effective NN interactions is also a remaining problem to be solved.

Appendix A: Comparison between the folding potential approximation and the microscopic calculation of V_0

In the present calculation, the Λ wave functions are obtained by folding the spin-independent central term (V_0) of the ΛN interactions. The nuclear density matrix in the exchange potential is approximated with the den-

sity matrix expansion in the local density approximation [63]. We discuss here its validity of the approximation for energy spectra in ${}^7_\Lambda\text{Li}$.

In Table X, the approximated Λ -potential energy $\langle \phi_{\Lambda,0} | U_0(\rho_N^{I^\pi}) | \phi_{\Lambda,0} \rangle$ is compared with the microscopically calculated energy $\langle \Psi_{\Lambda Z}^A(J^\pi) | V_0 | \Psi_{\Lambda Z}^A(J^\pi) \rangle$. Here, $\Psi_{\Lambda Z}^A(J^\pi) = [\Psi_N(I_n^\pi) \phi_{\Lambda,0} \chi_\Lambda]_J$ is the microscopic A -body wave function for ${}^A_\Lambda Z$ and $\phi_{\Lambda,0}(\rho_N^{I^\pi}; r)$ is fixed to be that obtained by the folding potential model. It should be noted that, in the folding potential model, the nuclear density $\rho_N^{I^\pi}$ is defined for intrinsic wave functions of $A-1$ Z without the cm motion, and the Λ recoil effect is properly taken into account. However, the microscopic A -body wave function $\Psi_{\Lambda Z}^A$ contains the cm motion. For consistency, we also perform the approximated and the microscopic calculations of the Λ -potential energy by using the nuclear density $\rho_{N,\text{cm}}^{I^\pi}$ with the cm motion instead of $\rho_N^{I^\pi}$ without the cm motion. As shown in the table, errors of the approximation are only $< 7\%$ and $< 2\%$ in the Λ -potential energy calculated with $\rho_N^{I^\pi}$ and $\rho_{N,\text{cm}}^{I^\pi}$, respectively. Moreover, the errors are almost state-independent and give only global shifts meaning that the approximation gives minor effect to energy spectra.

Appendix B: Core rearrangement effect to spin-doublet splitting energy

In the present perturbative treatment of the spin-dependent part (V_1) of the ΛN interactions, the nuclear spin rearrangement is ignored. Generally, its effects are expected to be minor because V_1 is relatively weak compared with the NN interactions and also the spin-independent part (V_0) of the ΛN interactions. Possible exception is the case that two energy levels with the same J^π eventually exist close to each other. In order to see nuclear spin rearrangement effects, we calculate the energy spectra of ${}^8_\Lambda\text{Li}$, ${}^{10}_\Lambda\text{Be}$, ${}^{12}_\Lambda\text{C}$, and ${}^{16}_\Lambda\text{O}$ with the AMD by diagonalization of the full Hamiltonian including V_0 and V_1 terms of the ΛN interactions. The spin-doublet splittings calculated with and without the rearrangement are compared in Table XI. One can see that the rearrangement effect is minor in most of states.

Acknowledgments

The computational calculations of this work were performed by using the supercomputer in the Yukawa Institute for theoretical physics, Kyoto University. This work was supported by Grant-in-Aid for Scientific Research (C) (No. 26400270), Grants-in-Aid for Young Scientists (B) (No. 15K17671), and Grant-in-Aid for JSPS Research Fellow (No. 16J05297) from Japan Society for the Promotion of Science(JSPS).

-
- [1] O. Hashimoto and H. Tamura, *Prog. Part. Nucl. Phys.* **57**, 564 (2006).
- [2] H. Tamura, *Prog. Theor. Phys. Suppl.* **185**, 315 (2010).
- [3] H. Tamura *et al.*, *Nucl. Phys. A* **914**, 99 (2013).
- [4] S. B. Yang *et al.*, *JPS Conf. Proc.* **17**, 012004 (2017).
- [5] T. Motoba, H. Bandō and K. Ikeda, *Prog. Theor. Phys.* **70**, 189 (1983).
- [6] T. Motoba, H. Bandō, K. Ikeda and T. Yamada, *Prog. Theor. Phys. Suppl.* **81** 42 (1985).
- [7] T. I. Yamada, K. Ikeda, H. Bando and T. Motoba, *Prog. Theor. Phys.* **73**, 397 (1985).
- [8] Y. W. Yu, T. Motoba and H. Bando, *Prog. Theor. Phys.* **76**, 861 (1986).
- [9] E. Hiyama, M. Kamimura, T. Motoba, T. Yamada and Y. Yamamoto, *Phys. Rev. C* **53**, 2075 (1996).
- [10] E. Hiyama, M. Kamimura, T. Motoba, T. Yamada and Y. Yamamoto, *Prog. Theor. Phys.* **97**, 881 (1997).
- [11] E. Hiyama, M. Kamimura, K. Miyazaki and T. Motoba, *Phys. Rev. C* **59**, 2351 (1999).
- [12] E. Hiyama, M. Kamimura, T. Motoba, T. Yamada and Y. Yamamoto, *Phys. Rev. Lett.* **85**, 270 (2000).
- [13] E. Hiyama, M. Kamimura, T. Motoba, T. Yamada and Y. Yamamoto, *Phys. Rev. C* **66**, 024007 (2002).
- [14] E. Hiyama, Y. Yamamoto, T. A. Rijken and T. Motoba, *Phys. Rev. C* **74**, 054312 (2006).
- [15] E. Hiyama, T. Motoba, T. A. Rijken and Y. Yamamoto, *Prog. Theor. Phys. Suppl.* **185**, 1 (2010).
- [16] E. Hiyama and Y. Yamamoto, *Prog. Theor. Phys.* **128**, 105 (2012).
- [17] E. Cravo, A. C. Fonseca and Y. Koike, *Phys. Rev. C* **66**, 014001 (2002).
- [18] V. M. Suslov, I. Filikhin and B. Vlahovic, *J. Phys. G* **30**, 513 (2004).
- [19] M. Shoen and Sonika, *Phys. Rev. C* **79**, 054321 (2009).
- [20] Y. Zhang, E. Hiyama and Y. Yamamoto, *Nucl. Phys. A* **881**, 288 (2012).
- [21] Y. Funaki, T. Yamada, E. Hiyama, B. Zhou and K. Ikeda, *Prog. Theor. Exp. Phys.* **2014**, no. 11, 113D01 (2014).
- [22] Y. Funaki, M. Isaka, E. Hiyama, T. Yamada and K. Ikeda, *Phys. Lett. B* **773**, 336 (2017).
- [23] A. Gal, J. M. Soper and R. H. Dalitz, *Annals Phys.* **63**, 53 (1971).
- [24] A. Gal, J. M. Soper and R. H. Dalitz, *Annals Phys.* **72**, 445 (1972).
- [25] A. Gal, J. M. Soper and R. H. Dalitz, *Annals Phys.* **113**, 79 (1978).
- [26] D. J. Millener, *Nucl. Phys. A* **804**, 84 (2008).
- [27] D. J. Millener, *Nucl. Phys. A* **835**, 11 (2010).
- [28] D. J. Millener, *Nucl. Phys. A* **881**, 298 (2012).
- [29] N. Guleria, S. K. Dhiman and R. Shyam, *Nucl. Phys. A* **886**, 71 (2012).
- [30] I. Vidana, A. Polls, A. Ramos and H.-J. Schulze, *Phys. Rev. C* **64**, 044301 (2001).
- [31] X. R. Zhou, H.-J. Schulze, H. Sagawa, C. X. Wu and E. G. Zhao, *Phys. Rev. C* **76**, 034312 (2007).
- [32] M. T. Win and K. Hagino, *Phys. Rev. C* **78**, 054311 (2008).
- [33] M. T. Win, K. Hagino and T. Koike, *Phys. Rev. C* **83**, 014301 (2011).
- [34] B. N. Lu, E. G. Zhao and S. G. Zhou, *Phys. Rev. C* **84**, 014328 (2011).
- [35] H. Mei, K. Hagino, J. M. Yao and T. Motoba, *Phys. Rev. C* **90**, 064302 (2014).
- [36] H. Mei, K. Hagino, J. M. Yao and T. Motoba, *Phys. Rev. C* **91**, 064305 (2015).
- [37] H. Mei, K. Hagino, J. M. Yao and T. Motoba, *Phys. Rev. C* **93**, no. 4, 044307 (2016).
- [38] H.-J. Schulze and E. Hiyama, *Phys. Rev. C* **90**, no. 4, 047301 (2014).
- [39] M. Isaka, M. Kimura, A. Dote and A. Ohnishi, *Phys. Rev. C* **83**, 044323 (2011).
- [40] M. Isaka and M. Kimura, *Phys. Rev. C* **92**, no. 4, 044326 (2015).
- [41] H. Homma, M. Isaka and M. Kimura, *Phys. Rev. C* **91**, no. 1, 014314 (2015).
- [42] M. Isaka, Y. Yamamoto and T. A. Rijken, *Phys. Rev. C* **94**, no. 4, 044310 (2016).
- [43] M. Isaka, Y. Yamamoto and T. A. Rijken, *Phys. Rev. C* **95**, no. 4, 044308 (2017).
- [44] R. Wirth, D. Gazda, P. Navrátil, A. Calci, J. Langhammer and R. Roth, *Phys. Rev. Lett.* **113**, no. 19, 192502 (2014).
- [45] T. A. Rijken, M. M. Nagels and Y. Yamamoto, *Nucl. Phys. A* **835**, 160 (2010).
- [46] T. A. Rijken, M. M. Nagels and Y. Yamamoto, *Prog. Theor. Phys. Suppl.* **185**, 14 (2010).
- [47] Y. Yamamoto, T. Motoba and T. A. Rijken, *Prog. Theor. Phys. Suppl.* **185**, 72 (2010).
- [48] Y. Kanada-En'yo, H. Horiuchi and A. Ono, *Phys. Rev. C* **52**, 628 (1995).
- [49] Y. Kanada-En'yo and H. Horiuchi, *Phys. Rev. C* **52**, 647 (1995).
- [50] Y. Kanada-En'yo and H. Horiuchi, *Prog. Theor. Phys. Suppl.* **142**, 205 (2001).
- [51] Y. Kanada-En'yo, M. Kimura and A. Ono, *Prog. Theor. Exp. Phys.* **2012** 01A202 (2012).
- [52] Y. Kanada-En'yo, *Phys. Rev. Lett.* **81**, 5291 (1998).
- [53] Y. Kanada-En'yo and T. Suhara, *Phys. Rev. C* **89**, no. 4, 044313 (2014).
- [54] Y. Kanada-En'yo, H. Morita and F. Kobayashi, *Phys. Rev. C* **91**, 054323 (2015).
- [55] Y. Kanada-En'yo, arXiv:1709.03375 [nucl-th].
- [56] D. L. Hill and J. A. Wheeler, *Phys. Rev.* **89**, 1102 (1953).
- [57] J. J. Griffin and J. A. Wheeler, *Phys. Rev.* **108**, 311 (1957).
- [58] Y. Kanada-En'yo, arXiv:1801.01259 [nucl-th].
- [59] D. M. Brink, *Proc. Int. School of Physics Enrico Fermi, Course 36*, Varenna, ed. C. Bloch (Academic Press, New York, 1966).
- [60] Y. Kanada-En'yo, *Phys. Rev. C* **94**, 024326 (2016).
- [61] T. Suhara and Y. Kanada-En'yo, *Phys. Rev. C* **91**, no. 2, 024315 (2015).
- [62] Y. Kanada-En'yo and F. Kobayashi, *Phys. Rev. C* **90**, no. 5, 054332 (2014).
- [63] J. W. Negele and D. Vautherin, *Phys. Rev. C* **11**, 1031 (1975).
- [64] M. Kamimura, *Phys. Rev. A* **38**, 621 (1988).
- [65] E. Hiyama, Y. Kino and M. Kamimura, *Prog. Part. Nucl. Phys.* **51**, 223 (2003).
- [66] A. B. Volkov, *Nucl. Phys.* **74**, 33 (1965).
- [67] N. Yamaguchi, T. Kasahara, S. Nagata and Y. Akaishi, *Prog. Theor. Phys.* **62**, 1018 (1979); R. Tamagaki, *Prog.*

- Theor. Phys. **39**, 91 (1968).
- [68] F. Ajzenberg-Selove, Nucl. Phys. A **506**, 1 (1990).
 - [69] D. R. Tilley, C. M. Cheves, J. L. Godwin, G. M. Hale, H. M. Hofmann, J. H. Kelley, C. G. Sheu and H. R. Weller, Nucl. Phys. A **708**, 3 (2002).
 - [70] D. R. Tilley, J. H. Kelley, J. L. Godwin, D. J. Millener, J. E. Purcell, C. G. Sheu and H. R. Weller, Nucl. Phys. A **745**, 155 (2004).
 - [71] J. H. Kelley, E. Kwan, J. E. Purcell, C. G. Sheu and H. R. Weller, Nucl. Phys. A **880**, 88 (2012).
 - [72] I. Angeli, and K. P. Marinova, Atom. Data Nucl. Data Tabl. **99**, 69 (2013).
 - [73] M. Jurič *et al.*, Nucl. Phys. B **52**, 1 (1973).
 - [74] D. H. Davis, Nucl. Phys. A **547**, 369C (1992).
 - [75] D. H. Davis, Nucl. Phys. A **754**, 3 (2005).
 - [76] S. Ajimura *et al.* [KEK-PS E336 Collaboration], Nucl. Phys. A **639**, 93 (1998).
 - [77] L. Tang *et al.* [HKS Collaboration], Phys. Rev. C **90**, 034320 (2014).
 - [78] R. E. Chrien *et al.*, Phys. Rev. C **41**, 1062 (1990).
 - [79] K. Tanida *et al.*, Phys. Rev. Lett. **86**, 1982 (2001).
 - [80] S. Ajimura *et al.*, Phys. Rev. Lett. **86**, 4255 (2001).
 - [81] H. Kohri *et al.* [AGS-E929 Collaboration], Phys. Rev. C **65**, 034607 (2002).
 - [82] H. Akikawa *et al.*, Phys. Rev. Lett. **88**, 082501 (2002).
 - [83] Y. Miura *et al.*, Nucl. Phys. A **754**, 75 (2005).
 - [84] M. Ukai *et al.* [E930'01 Collaboration], Phys. Rev. C **73**, 012501 (2006).
 - [85] M. Ukai *et al.* [BNL E930 Collaboration], Phys. Rev. C **77**, 054315 (2008).
 - [86] Y. Ma *et al.*, Nucl. Phys. A **835**, 422 (2010).
 - [87] K. Hosomi *et al.*, Prog. Theor. Exp. Phys. **2015**, no. 8, 081D01 (2015).
 - [88] A. Umeya, private communication.
 - [89] T. Motoba, JPS Conf. Proc. **17**, 011003 (2017).
 - [90] A. Umeya and T. Motoba, Nucl. Phys. A **954**, 242 (2016).

TABLE III: Nuclear properties of excitation energies (E_x [MeV]), magnetic moments (μ [μ_N]), and intrinsic-spin and orbital angular momentum expectation values in ^{A-1}Z . The AMD and AMD' results are shown. For excitation energies, The CL result of E_x is also shown. For ^{18}F , the CL result is shown. The experimental data are from Refs. [68–71]

^{A-1}Z	I^π	exp E_x	CL E_x	AMD E_x	AMD' E_x	exp μ	AMD				AMD'			
							μ	$\langle S_z \rangle$	$\langle S^2 \rangle$	$\langle L^2 \rangle$	μ	$\langle S_z \rangle$	$\langle S^2 \rangle$	$\langle L^2 \rangle$
^6Li	3^+	2.186	2.08	2.00		—	1.88	1.00	2.00	6.00				
^6Li	1^+_{gs}					0.822	0.88	1.00	2.00	0.00				
^7Li	$7/2^-$	4.630	4.75	4.88		—	3.74	0.52	0.82	11.92				
^7Li	$5/2^-$	6.680	unbound	7.17		—	-0.99	-0.35	0.77	11.96				
^7Li	$3/2^-_{\text{gs}}$					3.256	3.13	0.50	0.79	2.04				
^7Li	$1/2^-$	0.478	0.49	0.79		—	-0.74	-0.16	0.78	2.02				
^8Be	2^+	3.040	3.11	3.34	3.34	—	1.00	0.00	0.02	6.01	1.00	0.00	0.01	6.01
^8Be	0^+_{gs}					—	0.00	0.00	0.02	0.02	0.00	0.00	0.02	0.02
^9Be	$5/2^-$	2.429	2.02	2.27	2.22	—	-0.78	0.44	0.76	6.46	-0.89	0.46	0.76	6.29
^9Be	$3/2^-_{\text{gs}}$					-1.178	-1.13	0.37	0.76	2.64	-1.23	0.40	0.76	2.52
^9Be	$1/2^-$	2.780	2.20	3.23	2.53	—	0.83	-0.17	0.76	2.00	0.84	-0.17	0.75	2.00
^{10}Be	2^+	3.368	3.21	3.67	3.51	—	1.11	0.11	0.75	6.09	0.83	0.05	0.32	6.03
^{10}Be	0^+_{gs}					—	0.00	0.00	0.74	0.74	0.00	0.00	0.37	0.37
^{10}B	3^+_{gs}					1.801	1.82	0.85	2.07	7.25	1.83	0.86	2.03	7.14
^{10}B	1^+	0.718	1.21	4.15	1.87	0.63(2)	0.76	0.69	2.01	1.24	0.77	0.70	2.01	1.21
^{11}B	$5/2^-$	4.445	4.66	3.98	2.87	—	3.77	0.51	1.15	6.37	3.81	0.49	0.91	6.24
^{11}B	$3/2^-_{\text{gs}}$					2.689	2.32	0.26	1.26	3.74	2.27	0.25	0.95	3.43
^{11}B	$1/2^-$	2.125	2.79	2.77	1.22	—	-0.61	-0.16	0.98	2.22	-0.60	-0.16	0.87	2.11
^{11}B	$3/2^-_2$	5.020	5.57	6.09	4.08	—	0.75	-0.01	1.00	4.75	0.69	-0.04	0.85	4.79
^{11}C	$5/2^-$	4.319	4.50	3.87	2.84	—	-0.88	0.50	1.14	6.38	-0.93	0.49	0.90	6.24
^{11}C	$3/2^-_{\text{gs}}$					-0.964	-0.63	0.26	1.25	3.74	-0.58	0.26	0.94	3.41
^{11}C	$1/2^-$	2.000	2.62	2.64	1.16	—	0.99	-0.16	0.97	2.21	0.98	-0.16	0.86	2.10
^{11}C	$3/2^-_2$	4.804	5.35	5.91	4.01	—	0.76	-0.01	0.99	4.75	0.80	-0.04	0.84	4.79
^{12}C	2^+	4.439	4.47	4.70	6.07	—	1.03	0.06	0.50	6.14	1.00	0.03	0.22	6.05
^{12}C	0^+_{gs}					—	0.00	0.00	0.95	0.95	0.00	0.00	0.28	0.28
^{15}O	$3/2^-$	6.176	5.65	9.88	0.96	—	-1.82	0.49	0.81	2.11	-1.83	0.49	0.79	2.09
^{15}O	$1/2^-_{\text{gs}}$					0.719	0.64	-0.16	0.83	2.06	0.64	-0.16	0.81	2.05
^{A-1}Z	I^π	exp E_x	CL E_x			exp μ	CL							
^{18}F	5^+	1.124	0.94			2.86(3)	μ	$\langle S_z \rangle$	$\langle S^2 \rangle$	$\langle L^2 \rangle$				
^{18}F	3^+	0.937	0.92			1.77(12)	2.88	0.99	2.00	20.00				
^{18}F	1^+_{gs}					—	1.85	0.93	1.95	6.54				
							0.81	0.81	1.94	6.00				

TABLE IV: Proton radii in ^{A-1}Z nuclei obtained by the CL and AMD calculations together with the experimental data. The experimental values of proton radii are reduced from charge radii [72].

^{A-1}Z	CL	AMD	exp
	R_p [fm]	R_p [fm]	R_p [fm]
^6Li	2.56	2.17	2.452
^7Li	2.43	2.16	2.307
^8Be	3.37	2.42	—
^9Be	2.60	2.37	2.384
^9B	2.86	2.52	—
^{10}B	2.39	2.26	2.281
^{11}B	2.30	2.18	2.263
^{11}C	2.36	2.24	—
^{12}C	2.35	2.16	2.326
^{15}O	2.58	2.35	—
^{18}F	2.74	—	—

TABLE V: The averaged Λ binding energies ($\bar{B}_{\Lambda,0}$ [MeV]), rms radii of the Λ distribution (r_Λ [fm]), mean k_F values ($\langle k_F \rangle_\Lambda$ [fm $^{-1}$]), and rms radii of nuclear matter distribution (R_N [fm]) in ${}^A_\Lambda Z$ for core ${}^{A-1}Z(I^\pi)$ states. The results obtained by the CL and AMD calculations with the spin-independent ΛN interactions (V_0) are shown. The experimental Λ binding energies (B_Λ [MeV]) [1, 73–77] and the spin-averaged values (\bar{B}_Λ [MeV]) determined from spectroscopic studies [2, 77] are also listed.

${}^A_\Lambda Z$	(I^π)	CL				AMD				exp	
		$\bar{B}_{\Lambda,0}$	r_Λ	$\langle k_F \rangle_\Lambda$	R_N	$\bar{B}_{\Lambda,0}$	r_Λ	$\langle k_F \rangle_\Lambda$	R_N	B_Λ	\bar{B}_Λ
${}^7_\Lambda\text{Li}$	(3^+)	5.93	2.54	0.98	2.13	5.96	2.57	0.98	2.06	—	—
${}^7_\Lambda\text{Li}$	(1^+_{gs})	5.35	2.64	0.93	2.32	5.66	2.63	0.94	2.17	5.58(3)	5.12(3)
${}^8_\Lambda\text{Li}$	$(7/2^-)$	7.02	2.48	0.99	2.25	6.88	2.53	0.99	2.21	—	—
${}^8_\Lambda\text{Li}$	$(5/2^-)$	6.15	2.56	0.95	2.39	6.74	2.56	0.97	2.25	—	—
${}^8_\Lambda\text{Li}$	$(3/2^-_{\text{gs}})$	6.68	2.55	0.96	2.34	6.73	2.56	0.97	2.25	—	—
${}^8_\Lambda\text{Li}$	$(1/2^-)$	6.48	2.58	0.94	2.39	6.68	2.57	0.97	2.26	—	—
${}^9_\Lambda\text{Be}$	(2^+)	5.15	2.58	0.94	2.59	7.41	2.58	0.95	2.42	—	—
${}^9_\Lambda\text{Be}$	(0^+_{gs})	6.53	2.59	0.93	2.57	7.42	2.57	0.96	2.41	6.71(4)	—
${}^{10}_\Lambda\text{Be}$	$(5/2^-)$	7.96	2.52	0.99	2.55	8.15	2.55	0.98	2.52	—	—
${}^{10}_\Lambda\text{Be}$	$(3/2^-_{\text{gs}})$	8.06	2.51	0.99	2.54	8.20	2.54	0.98	2.50	8.55(18)	—
${}^{10}_\Lambda\text{Be}$	$(1/2^-)$	7.33	2.60	0.95	2.71	7.80	2.60	0.95	2.60	—	—
${}^{11}_\Lambda\text{Be}$	(2^+)	9.10	2.45	1.07	2.37	9.02	2.45	1.10	2.22	—	—
${}^{11}_\Lambda\text{Be}$	(0^+_{gs})	9.01	2.47	1.06	2.39	9.04	2.45	1.10	2.22	—	—
${}^{11}_\Lambda\text{B}$	(3^+_{gs})	9.31	2.44	1.08	2.34	9.34	2.43	1.09	2.26	10.24(5)	10.09(5)
${}^{11}_\Lambda\text{B}$	(1^+)	8.54	2.53	1.01	2.53	8.71	2.52	1.03	2.44	—	—
${}^{12}_\Lambda\text{B}$	$(5/2^-)$	9.46	2.47	1.07	2.45	9.67	2.43	1.13	2.25	—	—
${}^{12}_\Lambda\text{B}$	$(3/2^-_{\text{gs}})$	10.06	2.40	1.13	2.29	9.76	2.42	1.14	2.21	11.38(2)	11.28(2)
${}^{12}_\Lambda\text{B}$	$(1/2^-)$	9.49	2.47	1.07	2.45	9.61	2.44	1.12	2.28	—	—
${}^{12}_\Lambda\text{B}$	$(3/2^-_2)$	9.21	2.50	1.05	2.51	9.55	2.45	1.11	2.30	—	—
${}^{12}_\Lambda\text{C}$	$(5/2^-)$	9.51	2.47	1.07	2.46	9.65	2.44	1.12	2.26	—	—
${}^{12}_\Lambda\text{C}$	$(3/2^-_{\text{gs}})$	10.14	2.40	1.13	2.30	9.73	2.42	1.14	2.22	10.76(19)	10.65(19)
${}^{12}_\Lambda\text{C}$	$(1/2^-)$	9.55	2.47	1.07	2.46	9.58	2.45	1.11	2.29	—	—
${}^{12}_\Lambda\text{C}$	$(3/2^-_2)$	9.25	2.50	1.05	2.53	9.53	2.46	1.11	2.31	—	—
${}^{13}_\Lambda\text{C}$	(2^+)	10.03	2.46	1.10	2.44	9.94	2.43	1.17	2.21	—	—
${}^{13}_\Lambda\text{C}$	(0^+_{gs})	10.44	2.41	1.15	2.31	9.99	2.42	1.19	2.16	11.69(12)	—
${}^{16}_\Lambda\text{O}$	$(3/2^-)$	11.53	2.47	1.13	2.61	11.48	2.43	1.20	2.38	—	—
${}^{16}_\Lambda\text{O}$	$(1/2^-_{\text{gs}})$	11.71	2.45	1.15	2.57	11.57	2.42	1.22	2.32	12.42(5)	12.42(5)
${}^{19}_\Lambda\text{F}$	(5^+)	12.65	2.48	1.17	2.70	—	—	—	—	—	—
${}^{19}_\Lambda\text{F}$	(3^+)	12.70	2.47	1.18	2.73	—	—	—	—	—	—
${}^{19}_\Lambda\text{F}$	(1^+_{gs})	12.78	2.47	1.17	2.74	—	—	—	—	—	—

TABLE VI: Spin-doublet splittings in ${}^A_\Lambda Z$ for core ${}^{A-1}Z(I^\pi)$ states obtained by the AMD calculation with the original (ESC08a) and modified (ESC08a-msd) spin dependences of the ΛN interactions. The Δ_σ , S_Λ , T contributions as well as the total splitting energies are listed. The experimental values of the splittings from Refs.[2, 4, 77–87] are also shown. ^aFor the experimental value in ${}^8_\Lambda\text{Li}$, the 442 keV γ -ray was tentatively attributed to the transitions in ${}^8_\Lambda\text{Li}$ and ${}^8_\Lambda\text{Be}$ [78].

${}^A_\Lambda Z$	(I^π)	$J^\pi_>$	$J^\pi_<$	Modified (ESC08a-msd)				original (ESC08a)		exp
				Δ_σ	S_Λ	T	Total	Δ_σ	Total	
${}^7_\Lambda\text{Li}$	(3^+)	$7/2^+$	$5/2^+$	0.474	-0.018	-0.061	0.396	-0.399	-0.427	0.471
${}^7_\Lambda\text{Li}$	(1^+_{gs})	$3/2^+$	$1/2^+$	0.522	0.000	0.001	0.523	-0.423	-0.422	0.692
${}^8_\Lambda\text{Li}$	$(7/2^-)$	4^-	3^-	0.291	-0.026	-0.045	0.219	-0.195	-0.229	-
${}^8_\Lambda\text{Li}$	$(5/2^-)$	3^-	2^-	-0.126	-0.026	0.041	-0.111	0.136	0.117	-
${}^8_\Lambda\text{Li}$	$(3/2^-_{\text{gs}})$	2^-	1^-	0.286	-0.010	-0.024	0.252	-0.204	-0.218	0.442 ^a
${}^8_\Lambda\text{Li}$	$(1/2^-)$	1^-	0^-	-0.117	-0.010	0.095	-0.032	0.089	0.095	-
${}^9_\Lambda\text{Be}$	(2^+)	$5/2^+$	$3/2^+$	-0.002	-0.018	-0.003	-0.023	-0.007	-0.025	-0.043
${}^{10}_\Lambda\text{Be}$	$(5/2^-)$	3^-	2^-	0.206	-0.020	0.010	0.196	-0.106	-0.124	-
${}^{10}_\Lambda\text{Be}$	$(3/2^-_{\text{gs}})$	2^-	1^-	0.192	-0.013	-0.021	0.159	-0.106	-0.122	-
${}^{10}_\Lambda\text{Be}$	$(1/2^-)$	1^-	0^-	-0.095	-0.011	0.099	-0.007	0.045	0.051	-
${}^{11}_\Lambda\text{Be}$	(2^+)	$5/2^+$	$3/2^+$	0.098	-0.018	0.004	0.084	-0.068	-0.086	-
${}^{11}_\Lambda\text{B}$	(3^+_{gs})	$7/2^+$	$5/2^+$	0.487	-0.020	-0.060	0.407	-0.374	-0.404	0.264
${}^{11}_\Lambda\text{B}$	(1^+)	$3/2^+$	$1/2^+$	0.408	-0.004	-0.044	0.360	-0.253	-0.264	0.505
${}^{12}_\Lambda\text{B}$	$(5/2^-)$	3^-	2^-	0.313	-0.020	0.059	0.352	-0.225	-0.235	-
${}^{12}_\Lambda\text{B}$	$(3/2^-_{\text{gs}})$	2^-	1^-	0.172	-0.014	-0.055	0.103	-0.129	-0.152	0.179
${}^{12}_\Lambda\text{B}$	$(1/2^-)$	1^-	0^-	-0.130	-0.011	0.131	-0.010	0.096	0.106	-
${}^{12}_\Lambda\text{B}$	$(3/2^-_2)$	2^-	1^-	0.021	-0.017	-0.049	-0.045	-0.012	-0.037	-
${}^{12}_\Lambda\text{C}$	$(5/2^-)$	3^-	2^-	0.313	-0.020	0.059	0.352	-0.225	-0.235	-
${}^{12}_\Lambda\text{C}$	$(3/2^-_{\text{gs}})$	2^-	1^-	0.175	-0.014	-0.055	0.106	-0.132	-0.155	0.161
${}^{12}_\Lambda\text{C}$	$(1/2^-)$	1^-	0^-	-0.131	-0.011	0.130	-0.012	0.096	0.107	-
${}^{12}_\Lambda\text{C}$	$(3/2^-_2)$	2^-	1^-	0.018	-0.017	-0.048	-0.047	-0.010	-0.035	-
${}^{13}_\Lambda\text{C}$	(2^+)	$5/2^+$	$3/2^+$	0.049	-0.019	0.034	0.064	-0.070	-0.083	-
${}^{16}_\Lambda\text{O}$	$(3/2^-)$	2^-	1^-	0.328	-0.012	-0.034	0.282	-0.147	-0.164	0.224
${}^{16}_\Lambda\text{O}$	$(1/2^-_{\text{gs}})$	1^-	0^-	-0.167	-0.011	0.184	0.006	0.099	0.119	0.026
${}^{19}_\Lambda\text{F}$	(5^+)	$11/2^+$	$9/2^+$	0.199	-0.019	-0.052	0.128	-0.372	-0.399	-
${}^{19}_\Lambda\text{F}$	(3^+)	$7/2^+$	$5/2^+$	0.219	-0.011	-0.031	0.177	-0.328	-0.344	-
${}^{19}_\Lambda\text{F}$	(1^+_{gs})	$3/2^+$	$1/2^+$	0.219	0.000	0.031	0.249	-0.356	-0.351	0.315

TABLE VII: Spin-doublet splittings in ${}^A_\Lambda Z$ for core ${}^{A-1}Z(I^\pi)$ states obtained by the AMD calculation with the ESC08a-msd compared with the experimental and SM calculations. The Δ_σ , S_Λ , T contributions, and total splittings are listed together with the Millener's SM calculation [28]. $\Lambda\Sigma$ and S_N contributions in the Millener's calculation are also shown. Other SM calculations are taken from Refs. [88–90]. Information of the experimental values is explained in the caption of Table VI.

${}^A_\Lambda Z$	(I^π)	$J^\pi_>$	$J^\pi_<$	Present				exp	SM Total	SM[28]					
				Δ_σ	S_Λ	T	Total			Total	Δ_σ	S_Λ	T	$\Lambda\Sigma$	S_N
${}^7_\Lambda\text{Li}$	(3^+)	$7/2^+$	$5/2^+$	0.474	-0.018	-0.061	0.396	0.471		0.494	0.557	-0.032	-0.071	0.074	-0.008
${}^7_\Lambda\text{Li}$	(1^+_{gs})	$3/2^+$	$1/2^+$	0.522	0.000	0.001	0.523	0.692		0.693	0.628	-0.001	-0.009	0.072	-0.004
${}^8_\Lambda\text{Li}$	$(7/2^-)$	4^-	3^-	0.291	-0.026	-0.045	0.219	-		0.307	-	-	-	-	-
${}^8_\Lambda\text{Li}$	$(3/2^-_{\text{gs}})$	2^-	1^-	0.286	-0.010	-0.024	0.252	0.442 ^a		0.445	0.393	-0.014	-0.023	0.149	-0.015
${}^8_\Lambda\text{Li}$	$(1/2^-)$	1^-	0^-	-0.117	-0.010	0.095	-0.032	-		0.006	-	-	-	-	-
${}^9_\Lambda\text{Be}$	(2^+)	$5/2^+$	$3/2^+$	-0.002	-0.018	-0.003	-0.023	-0.043		-0.044	0.014	-0.037	-0.028	0.008	0.000
${}^{10}_\Lambda\text{Be}$	$(5/2^-)$	3^-	2^-	0.206	-0.020	0.010	0.196	-	0.148[88]	0.103	0.172	-0.037	-0.010	-0.019	-0.005
${}^{10}_\Lambda\text{Be}$	$(3/2^-_{\text{gs}})$	2^-	1^-	0.192	-0.013	-0.021	0.159	-	0.165[88]	0.110	0.180	-0.022	-0.033	-0.010	-0.004
${}^{10}_\Lambda\text{Be}$	$(1/2^-)$	1^-	0^-	-0.095	-0.011	0.099	-0.007	-	-0.162[88]	0.026	-	-	-	-	-
${}^{11}_\Lambda\text{B}$	(3^+_{gs})	$7/2^+$	$5/2^+$	0.487	-0.020	-0.060	0.407	0.264		0.267	0.339	-0.037	-0.080	0.056	-0.010
${}^{11}_\Lambda\text{B}$	(1^+)	$3/2^+$	$1/2^+$	0.408	-0.004	-0.044	0.360	0.505		0.475	0.424	-0.003	-0.010	0.061	-0.044
${}^{12}_\Lambda\text{B}$	$(5/2^-)$	3^-	2^-	0.313	-0.020	0.059	0.352	-	0.389[89]	-	-	-	-	-	-
${}^{12}_\Lambda\text{B}$	$(3/2^-_{\text{gs}})$	2^-	1^-	0.172	-0.014	-0.055	0.103	0.179	0.186[89]	-	-	-	-	-	-
${}^{12}_\Lambda\text{B}$	$(1/2^-)$	1^-	0^-	-0.130	-0.011	0.131	-0.010	-	-0.664[89]	-	-	-	-	-	-
${}^{12}_\Lambda\text{B}$	$(3/2^-_2)$	2^-	1^-	0.021	-0.017	-0.049	-0.045	-	-0.122[89]	-	-	-	-	-	-
${}^{12}_\Lambda\text{C}$	$(3/2^-_{\text{gs}})$	2^-	1^-	0.175	-0.014	-0.055	0.106	0.161		0.153	0.175	-0.012	-0.042	0.061	-0.013
${}^{16}_\Lambda\text{O}$	$(3/2^-)$	2^-	1^-	0.328	-0.012	-0.034	0.282	0.224		0.248	0.207	-0.021	-0.041	0.092	0.001
${}^{16}_\Lambda\text{O}$	$(1/2^-_{\text{gs}})$	1^-	0^-	-0.167	-0.011	0.184	0.006	0.026		0.023	-0.123	-0.020	0.188	-0.033	0.001
${}^{19}_\Lambda\text{F}$	(5^+)	$11/2^+$	$9/2^+$	0.199	-0.019	-0.052	0.128	-	0.408[90]	-	-	-	-	-	-
${}^{19}_\Lambda\text{F}$	(3^+)	$7/2^+$	$5/2^+$	0.219	-0.011	-0.031	0.177	-	0.562[90]	0.196	-	-	-	-	-
${}^{19}_\Lambda\text{F}$	(1^+_{gs})	$3/2^+$	$1/2^+$	0.219	0.000	0.031	0.249	0.315	0.419[90]	0.305	-	-	-	-	-

TABLE VIII: NN interaction dependence of the spin-doublet splittings in ${}^A_\Lambda Z$ for core ${}^{A-1}Z(I^\pi)$ states. The results of the AMD and AMD' calculations with the ESC8a-msd interactions are shown. Information of the experimental values is explained in the caption of Table VI.

${}^A_\Lambda Z$	(I^π)	$J^\pi_>$	$J^\pi_<$	AMD				exp	AMD'			
				Δ_σ	S_Λ	T	Total		Δ_σ	S_Λ	T	Total
${}^9_\Lambda\text{Be}$	(2^+)	$5/2^+$	$3/2^+$	-0.002	-0.018	-0.003	-0.023	-0.043	-0.002	-0.018	-0.003	-0.023
${}^{10}_\Lambda\text{Be}$	$(5/2^-)$	3^-	2^-	0.206	-0.020	0.010	0.196	-	0.193	-0.020	0.015	0.188
${}^{10}_\Lambda\text{Be}$	$(3/2^-_{\text{gs}})$	2^-	1^-	0.192	-0.013	-0.021	0.159	-	0.189	-0.012	-0.018	0.159
${}^{10}_\Lambda\text{Be}$	$(1/2^-)$	1^-	0^-	-0.095	-0.011	0.099	-0.007	-	-0.095	-0.011	0.097	-0.009
${}^{11}_\Lambda\text{Be}$	(2^+)	$5/2^+$	$3/2^+$	0.098	-0.018	0.004	0.084	-	0.027	-0.020	0.013	0.019
${}^{11}_\Lambda\text{B}$	(3^+_{gs})	$7/2^+$	$5/2^+$	0.487	-0.020	-0.060	0.407	0.264	0.464	-0.021	-0.052	0.391
${}^{11}_\Lambda\text{B}$	(1^+)	$3/2^+$	$1/2^+$	0.408	-0.004	-0.044	0.360	0.505	0.433	-0.004	-0.043	0.387
${}^{12}_\Lambda\text{C}$	$(5/2^-)$	3^-	2^-	0.313	-0.020	0.059	0.352	-	0.282	-0.020	0.058	0.319
${}^{12}_\Lambda\text{C}$	$(3/2^-_{\text{gs}})$	2^-	1^-	0.175	-0.014	-0.055	0.106	0.161	0.166	-0.014	-0.054	0.098
${}^{12}_\Lambda\text{C}$	$(1/2^-)$	1^-	0^-	-0.131	-0.011	0.130	-0.012	-	-0.135	-0.011	0.128	-0.018
${}^{12}_\Lambda\text{C}$	$(3/2^-_2)$	2^-	1^-	0.018	-0.017	-0.048	-0.047	-	-0.009	-0.017	-0.047	-0.073
${}^{13}_\Lambda\text{C}$	(2^+)	$5/2^+$	$3/2^+$	0.049	-0.019	0.034	0.064	-	0.025	-0.019	0.020	0.026

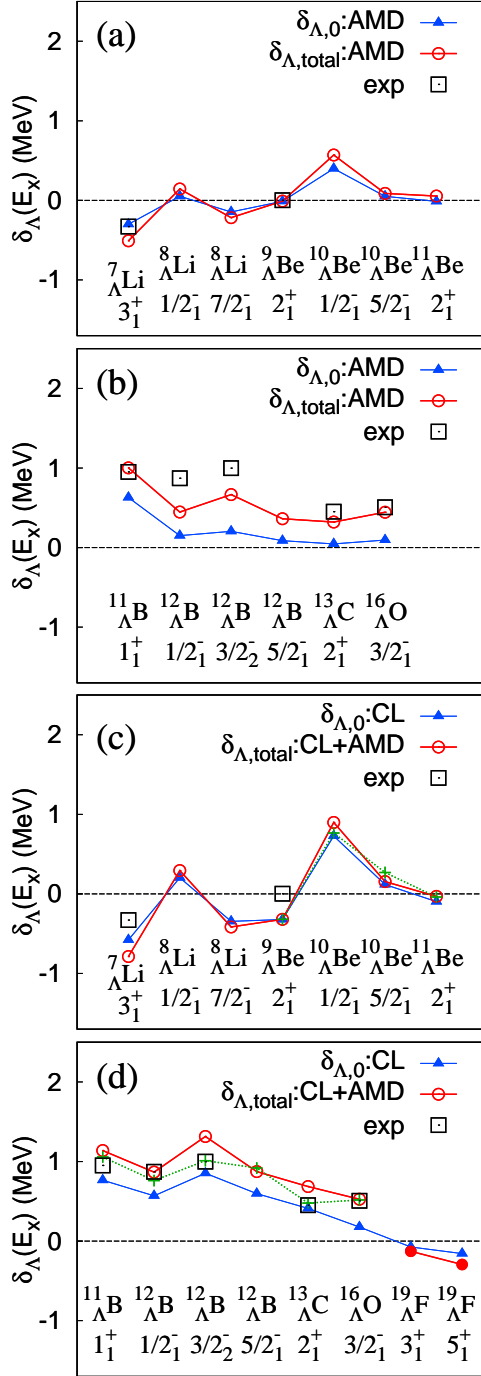


FIG. 2: (color online) Spin-averaged excitation energy shift $\delta_\Lambda(\bar{E}_x)$ in ${}^A_{\Lambda}Z$ for core ${}^{A-1}Z(I^\pi)$ states. (a)(b) The total energy shift ($\delta_\Lambda(\bar{E}_x) = \delta_\Lambda(\bar{E}_x) + \delta_{\Lambda,0}(\bar{E}_x)$) and the V_0 contribution ($\delta_{\Lambda,0}(\bar{E}_x)$) obtained by the AMD calculation. (c)(d) The total energy shift obtained by the CL+AMD calculation, and the V_0 contribution obtained by the CL calculation. In (c) and (d), the total energy shift obtained by the CL+AMD calculation is also shown by green cross points. For ${}^{19}_{\Lambda}\text{F}$, the total energy shift and V_0 contribution obtained by the CL calculation are plotted by red filled circles and blue filled triangles, respectively. Information of the experimental data is explained in the caption of Table IX.

TABLE IX: The spin-averaged excitation energy shifts ($\delta_\Lambda(\bar{E}_x)$), and S_N and V_0 contributions ($\delta_{\Lambda, S_N}(\bar{E}_x)$ and $\delta_{\Lambda, S_0}(\bar{E}_x)$) in ${}^A_\Lambda Z$ for core ${}^{A-1}Z(I^\pi)$ states. The AMD result of the S_N contribution, the AMD and CL results of the V_0 contribution, and the AMD and CL+AMD results of the total shifts are listed. The expectation values of the V_{S_N} term obtained by the AMD calculation are also shown. For ${}^{19}_\Lambda\text{F}$, the CL and CL $^{4\alpha}$ +CL results are shown. The experimental values are from Refs. [2, 77–87] except for ${}^{12}_\Lambda\text{C}(I^\pi = 1/2^-)$, ${}^{12}_\Lambda\text{C}(I^\pi = 3/2^-)$, and ${}^{13}_\Lambda\text{C}(I^\pi = 0^+)$. For ${}^{12}_\Lambda\text{C}(I^\pi = 1/2^-)$ and ${}^{13}_\Lambda\text{C}(I^\pi = 2^+)$, the excitation energy shifts for the ${}^{12}_\Lambda\text{C}(1^-)$ and ${}^{13}_\Lambda\text{C}(3/2^+)$ are shown. *For ${}^{12}_\Lambda\text{C}(I^\pi = 3/2^-)$, the averaged value of the observed excitation energies of ${}^{12}_\Lambda\text{C}(1^-)$ [87] and ${}^{12}_\Lambda\text{B}(2^-)$ [77] is deduced by assuming the same Coulomb shift between mirror states in ${}^{12}_\Lambda\text{C}$ - ${}^{12}_\Lambda\text{B}$ as that in ${}^{11}_\Lambda\text{C}$ - ${}^{11}_\Lambda\text{B}$. Energies are in MeV.

${}^A_\Lambda Z$	(I^π)	$\langle V_{S_N} \rangle$		$\delta_{\Lambda, S_N}(\bar{E}_x)$		$\delta_{\Lambda, 0}(\bar{E}_x)$		$\delta_\Lambda(\bar{E}_x)$		$\delta_\Lambda(\bar{E}_x)$ exp
		AMD	AMD	AMD	CL	AMD	CL+AMD	AMD	CL+AMD	
${}^7_\Lambda\text{Li}$	(3^+)	-0.22	-0.21	-0.30	-0.58	-0.51	-0.79	-0.51	-0.79	-0.329
${}^7_\Lambda\text{Li}$	(1^+_{gs})	-0.01	—	—	—	—	—	—	—	—
${}^8_\Lambda\text{Li}$	$(7/2^-)$	-0.15	-0.07	-0.15	-0.34	-0.22	-0.42	-0.22	-0.42	—
${}^8_\Lambda\text{Li}$	$(3/2^-_{\text{gs}})$	-0.08	—	—	—	—	—	—	—	—
${}^8_\Lambda\text{Li}$	$(1/2^-)$	0.01	0.09	0.05	0.20	0.14	0.29	0.14	0.29	—
${}^9_\Lambda\text{Be}$	(2^+)	-0.03	0.00	-0.01	-0.32	-0.01	-0.32	-0.01	-0.32	0.002
${}^9_\Lambda\text{Be}$	(0^+_{gs})	-0.03	—	—	—	—	—	—	—	—
${}^{10}_\Lambda\text{Be}$	$(5/2^-)$	-0.11	0.04	0.05	0.10	0.09	0.14	0.09	0.14	—
${}^{10}_\Lambda\text{Be}$	$(3/2^-_{\text{gs}})$	-0.15	—	—	—	—	—	—	—	—
${}^{10}_\Lambda\text{Be}$	$(1/2^-)$	0.03	0.17	0.40	0.72	0.57	0.89	0.57	0.89	—
${}^{11}_\Lambda\text{Be}$	(2^+)	-0.41	0.07	-0.01	-0.10	0.05	-0.03	0.05	-0.03	—
${}^{11}_\Lambda\text{Be}$	(0^+_{gs})	-0.47	—	—	—	—	—	—	—	—
${}^{11}_\Lambda\text{B}$	(3^+_{gs})	-0.44	—	—	—	—	—	—	—	—
${}^{11}_\Lambda\text{B}$	(1^+)	-0.07	0.37	0.63	0.77	1.00	1.14	1.00	1.14	0.951
${}^{12}_\Lambda\text{C}$	$(5/2^-)$	-0.30	0.27	0.08	0.62	0.36	0.90	0.36	0.90	—
${}^{12}_\Lambda\text{C}$	$(3/2^-_{\text{gs}})$	-0.57	—	—	—	—	—	—	—	—
${}^{12}_\Lambda\text{C}$	$(1/2^-)$	-0.28	0.29	0.15	0.59	0.45	0.89	0.45	0.89	0.732(1 $^-$)
${}^{12}_\Lambda\text{C}$	$(3/2^-_2)$	-0.12	0.46	0.20	0.89	0.66	1.35	0.66	1.35	1.01*
${}^{13}_\Lambda\text{C}$	(2^+)	-0.40	0.27	0.05	0.41	0.32	0.69	0.32	0.69	0.451(3/2 $^+$)
${}^{13}_\Lambda\text{C}$	(0^+_{gs})	-0.67	—	—	—	—	—	—	—	—
${}^{16}_\Lambda\text{O}$	$(3/2^-)$	0.11	0.35	0.09	0.18	0.44	0.53	0.44	0.53	0.507
${}^{16}_\Lambda\text{O}$	$(1/2^-_{\text{gs}})$	-0.24	—	—	—	—	—	—	—	—
		CL	CL	CL	CL $^{4\alpha}$	CL	CL $^{4\alpha}$ + CL	CL	CL $^{4\alpha}$ + CL	
${}^{19}_\Lambda\text{F}$	(5^+)	-0.19	-0.14	-0.13	-0.16	-0.27	-0.29	-0.27	-0.29	—
${}^{19}_\Lambda\text{F}$	(3^+)	-0.11	-0.05	-0.04	-0.07	-0.10	-0.13	-0.10	-0.13	—
${}^{19}_\Lambda\text{F}$	(1^+_{gs})	-0.05	—	—	—	—	—	—	—	—

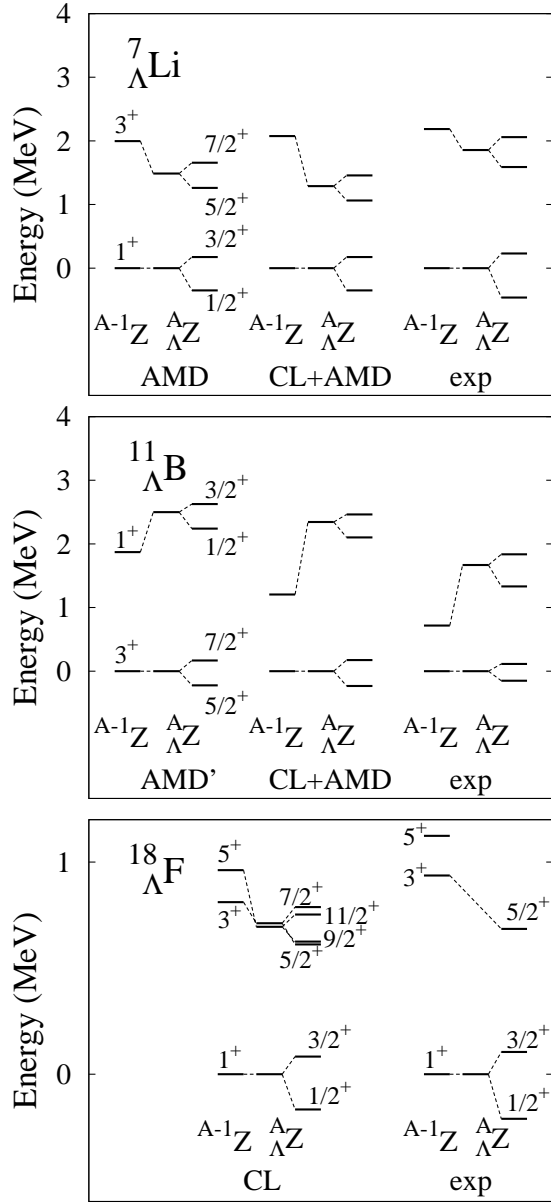


FIG. 3: Energy spectra in ${}^A_{\Lambda}Z$ for ${}^7_{\Lambda}\text{Li}$, ${}^{11}_{\Lambda}\text{B}$, and ${}^{18}_{\Lambda}\text{F}$ together with those in ${}^{A-1}Z$. The spectra in ${}^{A-1}Z$, the spin-averaged spectra in ${}^A_{\Lambda}Z$, and spectra in ${}^A_{\Lambda}Z$ are shown in the left, middle, and right columns, respectively. Experimental data are from Refs. [2, 4, 79, 83, 84, 86].

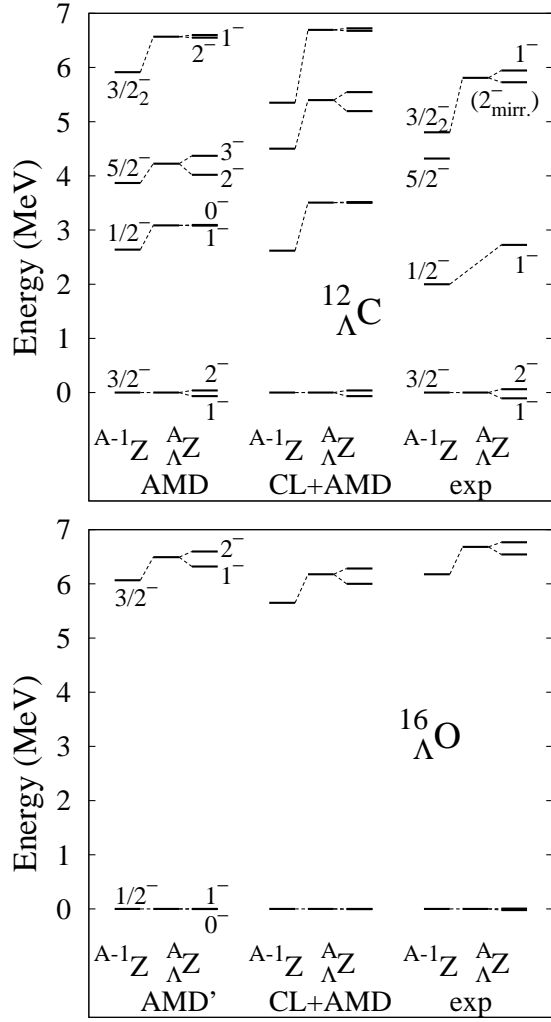


FIG. 4: Same as Fig. 4 but for $^{12}_{\Lambda}\text{C}$ and $^{16}_{\Lambda}\text{O}$. Experimental data are from Refs. [2, 85, 87]. As for the $^{12}_{\Lambda}\text{C}(J^{\pi} = 2^-)$ state for the core $^{11}\text{C}(3/2^-)$ state, the observed energy of the mirror state in $^{12}_{\Lambda}\text{B}$ [77] is plotted assuming the Coulomb shift between the mirror states in $^{12}_{\Lambda}\text{C}$ - $^{12}_{\Lambda}\text{B}$ is the same as that in ^{11}C - ^{11}B .

TABLE X: Comparison of the Λ potential energy in ${}^7_\Lambda\text{Li}(I^\pi = 1^+, 3^+)$ between the folding potential model approximation and the microscopic calculation. The energies calculated using the nuclear densities $\rho_N^{I^\pi}$ and $\rho_{N,\text{cm}}^{I^\pi}$ (without and with the cm motion) are shown. The difference between approximated and microscopic calculations is also shown. Energies are in MeV.

		approx.	micro.	diff.
${}^7_\Lambda\text{Li}(I^\pi = 1^+)$	ρ_N	-11.81	-11.04	-0.77
	$\rho_{N,\text{cm}}$	-11.10	-10.92	-0.18
${}^7_\Lambda\text{Li}(I^\pi = 3^+)$	ρ_N	-12.90	-12.06	-0.84
	$\rho_{N,\text{cm}}$	-12.16	-11.99	-0.17

TABLE XI: Spin-doublet splittings in ${}^A_\Lambda Z$ for core ${}^{A-1}Z(I^\pi)$ states calculated with and without nuclear spin rearrangement in the AMD calculation.

${}^A_\Lambda Z$	(I^π)	$J^\pi_>$	$J^\pi_<$	Splitting energy (MeV)	
				w/o	with
${}^8_\Lambda\text{Li}$	$(7/2^-)$	4^-	3^-	0.22	0.25
	$(5/2^-)$	3^-	2^-	-0.11	-0.10
	$(3/2^-_{\text{gs}})$	2^-	1^-	0.25	0.30
	$(1/2^-)$	1^-	0^-	-0.03	0.00
${}^{10}_\Lambda\text{Be}$	$(5/2^-)$	3^-	2^-	0.20	0.21
	$(3/2^-_{\text{gs}})$	2^-	1^-	0.16	0.17
	$(1/2^-)$	1^-	0^-	0.00	0.00
${}^{12}_\Lambda\text{C}$	$(5/2^-)$	3^-	2^-	0.35	0.36
	$(3/2^-_{\text{gs}})$	2^-	1^-	0.11	0.12
	$(1/2^-)$	1^-	0^-	-0.01	-0.01
	$(3/2^-_2)$	2^-	1^-	-0.05	-0.05
${}^{16}_\Lambda\text{O}$	$(3/2^-)$	2^-	1^-	0.28	0.28
	$(1/2^-_{\text{gs}})$	1^-	0^-	0.01	0.00